ANKARA YILDIRIM BEYAZIT UNIVERSITY

GRADUATE SCHOOL OF NATURAL AND APPLIED SCIENCES

NUMERICAL ANALYSIS OF THE THERMAL DISTRIBUTION OF A MACHINERY DRIVER'S CAB

M.Sc. Thesis by

Hazal KOYUNCU

Department of Mechanical Engineering

June, 2019

ANKARA

NUMERICAL ANALYSIS OF THE THERMAL DISTRIBUTION OF A MACHINERY DRIVER'S CAB

A Thesis Submitted to

The Graduate School of Natural and Applied Sciences of

Ankara Yıldırım Beyazıt University

In Partial Fulfillment of the Requirements for the Degree of Master of Science in Mechanical Engineering, Department of Mechanical Engineering

by

Hazal KOYUNCU

June, 2019

ANKARA

M.Sc. THESIS EXAMINATION RESULT FORM

We have read the thesis entitled **"NUMERICAL ANALYSIS OF THE THERMAL DISTRIBUTION OF A MACHINERY DRIVER'S CAB"** completed by **HAZAL KOYUNCU** under the supervision of **PROF. DR. VELİ ÇELİK** and we certify that in our opinion it is fully adequate, in scope and quality, as a thesis for the degree of Master of Science.

Prof. Dr. Veli ÇELİK

Supervisor

Prof. Dr. Adnan SÖZEN

Jury Member

Asst. Prof. Dr. Mustafa KAYA

Jury Member

Prof. Dr. Ergün ERASLAN

Director

Graduate School of Natural and Applied Sciences

I hereby declare that, in this thesis which has been prepared in accordance with the Thesis Writing Manual of Graduate School of Natural and Applied Sciences,

- All data, information and documents are obtained in the framework of academic and ethical rules,
- All information, documents and assessments are presented in accordance with scientific ethics and morals,
- All the materials that have been utilized are fully cited and referenced,
- No change has been made on the utilized materials,
- All the works presented are original,

and in any contrary case of above statements, I accept to renounce all my legal rights.

Date: **Signature:**

Name & Surname: Hazal KOYUNCU

ACKNOWLEDGMENTS

I wish to express my sincere gratitude to my thesis supervisor, Prof. Dr. Veli ÇELİK, for his excellent support and encouragement along this process. His guidance provided me with limitless motivation; without his assistance, this accomplishment would not have been possible.

I would also like to express my sincere thanks to HİDROMEK A.Ş. without their valuable contribution; it would not be possible to achieve the work required in this thesis.

Finally, I would like to thank my family. I am especially indebted to my mother, Zeliha KOYUNCU, for her unconditional support and continuous encouragement throughout writing my thesis.

2019, 17 June **Hazal KOYUNCU**

NUMERICAL ANALYSIS OF THE THERMAL DISTRIBUTION OF A MACHINERY DRIVER'S CAB

ABSTRACT

It is an indisputable fact that air conditioning systems play an important role in the vehicle. That is why today's vehicle manufacturers show high sensitivity to this issue in order to provide their customers with both comfortable travel and clean indoor air. In this thesis, the cooling problem in a machine driver's cab has been discussed. The cooling test has been carried out in a climatic test chamber. Airflow and temperature distributions have been observed in detail within the cab by this means. Computational mesh has been generated using ANSYS FLUENT meshing module. Commercial, Computational Fluid Dynamics (CFD) software FLUENT has been used to get numerical solutions. The necessary data have been collected during the air conditioning test conducted while the machinery was operating, and the measured data have been used as boundary conditions. The second numerical analysis has been made by considering the actual working conditions. Radiation effects have also been included in the numerical model in FLUENT. According to ISO 10263-4 standard, temperature measurements have been taken from specific points around the driver. Then the model verification has been done by comparing the CFD predictions with the test data. Consequently, an overall evaluation has been done, and proposals have been presented.

Keywords: HVAC, computational fluid dynamics, flow analysis, heat transfer, radiation modeling.

BİR İŞ MAKİNESİ KABİNİ İÇERİSİNDEKİ ISIL DAĞILIMIN SAYISAL ANALİZİ

ÖZ

İklimlendirme sistemlerinin araç içerisinde ne kadar önemli bir rol oynadığı tartışılmaz bir gerçektir. Bu yüzden günümüz araç üreticileri müşterilerine hem konforlu bir seyahat hem de temiz bir iç ortam havası sağlayabilmek için bu konuya büyük bir hassasiyet gösterirler. Bu çalışmada bir iş makinesi sürücü kabinindeki soğutma problemi ele alınmıştır. Soğutma testi klimatik bir test odasında yapılmıştır. Bu çalışma sayesinde hem kabin içerisindeki akış hızları hem de sıcaklık dağılımları gözlenmiştir. Geometrik modelin temizlenmesi ve akış modeli oluşturma çalışmaları Space Claim programında yapılmıştır. Sayısal ağ örme işlemi için ANSYS FLUENT Meshing programı kullanılmıştır. Numerik çözüm için kullanılan program ise ANSYS FLUENT paket programıdır. İş makinesi çalışır durumdayken yapılan klima testi sırasında gerekli veriler toplanmış ve analize sınır şartı olarak verilmiştir. İkinci sayısal analiz ise gerçek çalışma koşulları dikkate alınarak yapılmıştır. Isı transferinin yanı sıra FLUENT programı içerisindeki radyasyon modülü de aktif hale getirilerek, ışınımla radyasyonun etkileri incelenmiştir. ISO10263-4 standardına göre operatör çevresinden belli konumlarda sıcaklık ölçümleri alınmıştır. Bu noktaların test sıcaklık değerleriyle hesaplamalı akışkanlar dinamiğinden elde edilen değerler karşılaştırılarak model doğrulaması yapılmıştır. Sonuç olarak, genel bir değerlendirme yapılmış ve öneriler sunulmuştur.

Anahtar kelimeler: Hesaplamalı akışkanlar dinamiği (HAD), akış analizi, radyasyon modellemesi, ısı transferi.

CONTENTS

M.Sc. THESIS EXAMINATION RESULT FORM ii
ETHICAL DECLARATION iii
ACKNOWLEDGMENTS iv
ABSTRACT v
ÖZ vi
NOMENCLATURE ix
LIST OF TABLES xi
LIST OF FIGURES xii

CHAPTER 1 - INTRODUCTION 1
1.1 Draft of the Thesis 2
1.2 Purpose of the Thesis 2
1.3 Literature Review 3
1.3.1 Overview 3
1.3.2 Previous Studies 3
CHAPTER 2 – THEORETICAL BACKGROUND 10
2.1 Overview 10
2.2 Fluid Dynamics 10
2.2.1 Conservation of Mass 11
2.2.2 Conservation of Momentum 12
2.2.3 Conservation of Energy 13
2.3 Buoyancy Model 13
2.4 Types of Heat Transfer Mechanisms 15
2.4.1 Heat Conduction 15
2.4.2 Heat Convection 16
2.4.3 Radiation 17
2.5 COMPUTATIONAL FLUID DYNAMICS (CFD) 18
2.6 Turbulence 19
2.7 K-epsilon Realizable 21
2.8 Wall Functions 22
2.9 Solar Load Model 23

2.9.1 Solar Ray Tracing Algorithm 24
2.9.2 Surface to Surface Radiation Model (S2S) 25
CHAPTER 3 – NUMERICAL MODEL DEVELOPMENT 27
3.1 Overview 27
3.2 Creation Process of Model Geometry 27
3.3 Thermal Calculations 33
3.4 Numerical Setup 33
CHAPTER 4 - TEST CONDITIONS 39
4.1 Overview 39
4.2 Test Conditions of Driver's Cab 39
4.3 Test Equipment 40
4.3.1 Air Flow Meters 40
4.3.2 Type K Thermocouple 41
4.3.3 Pyranometer 42
CHAPTER 5 - RESULTS of NUMERICAL MODEL 43
5.1 Overview 43
5.2 Verification Process Steps 43
5.2.1 First analysis: Climatic Test Chamber 43
5.2.2 The Second Analysis: Real Working Conditions 60
CHAPTER 6 - CONCLUSION 63
REFERENCES 65
CURRICULUM VITAE 70

NOMENCLATURE

Symbol List

A	Area, m^2
c_p	Specific heat, J/K
E	Emissivity of surface
G	Incident radiation
G_k	Turbulence kinetic energy from the mean velocity gradients
G_b	Turbulence kinetic energy produced by buoyancy effect
h	Convection heat transfer coefficient, $W/(m^2K)$
k	Conduction heat transfer coefficient, $W/(m^2K)$
Nu	Nusselt number
P	Pressure, N/m^2
Pr	Prandtl number
q	Heat flux, $W \cdot m^{-2}$
R	Equivalent thermal resistance, $\Delta 1$ K
Re	Reynolds number
t	Time, s
T	Temperature, K
T_s	Temperature of surface, K
T_∞	Free stream temperature, K
u	Velocity, m/s
Ym	Expansion distribution in incompressible flow
y+	Dimensionless distance from the wall
β	Thermal expansion coefficient, $°C^{-1}$
ε	Emissivity
ρ	Density of fluid, kg/m^3
σ	Stefan-Boltzmann constant, W. m. K^{-4}
σ_k	Prandtl number for kinetic energy
σ_ε	Prandtl number for diffuse
τ	Transmitted radiation
μ	Dynamic viscosity of the fluid, $N \cdot s/m^2$
ν	Specific volume of fluid, m^3/kg
ϕ	Viscous dissipation function

Acronyms

CFD	Computational Fluid Mechanics
HAD	Hesaplamalı Akışkanlar Dinamiği
HVAC	Heating Ventilating and Air Conditioning
ISO	International Organization of Standardization
SAE	Society of Automotive Engineers
S2S	Surface to Surface Radiation Model
CPU	Central Processing Unit

LIST OF TABLES

Table 3.1 Average velocity and temperature values of air inlets for the first analysis 38

Table 3.2 Average velocity and temperature values of air inlets for second analysis 38

Table 5.1 Differences between temperature measurement and analysis results for the first analysis 45

Table 5.2 Differences between temperature measurement and analysis results for the second analysis 60

LIST OF FIGURES

Figure 1.1 Surface geometry and CFD model surface geometry 4
Figure 1.2 Surface geometry and CFD model surface geometry 4
Figure 1.3 3D simplified picture of the car cabin and vehicle test bench 5
Figure 3.1 The model geometry used in simulations 28
Figure 3.2 Detailed representation of air inlets in front of the cabin. 29
Figure 3.3 The position of the line in the cabin 30
Figure 3.4 Mesh independence study 30
Figure 3.5 Detailed mesh view on the cross-section 31
Figure 3.6 Inflation layer detailed representation 32
Figure 3.7 General view of the driver's cab mesh surfaces 32
Figure 3.8 Representation of the solar direction vector 36
Figure 3.9 Numbering order of fore air inlets 37
Figure 3.10 Order of numbering of the air inlets located in the back 37
Figure 4.1 Airflow meters 41
Figure 4.2 Type K Thermocouple [32] 42
Figure 4.3 Pyranometer [33] 42
Figure 5.1 Measurement point locations 44
Figure 5.2 Position of the number 1 cross section 46
Figure 5.3 The temperature distribution of number 1 cross section 47
Figure 5.4 The airspeed distribution of number 1 cross section 47
Figure 5.5 Position of the number 2 cross section 48
Figure 5.6 The temperature distribution of number 2 cross section 49
Figure 5.7 The airspeed distribution of number 2 cross section 49
Figure 5.8 Position of the number 3 cross section 50
Figure 5.9 The temperature distribution of number 3 cross section 51
Figure 5.10 The airspeed distribution of number 3 cross section 51
Figure 5.11 Position of the number 4 cross section 52
Figure 5.12 The temperature distribution of number 4 cross section 53
Figure 5.13 The airspeed distribution of number 4 cross section 53
Figure 5.14 Position of the number 5 cross section 54
Figure 5.15 Temperature values of the operator at the foot level 55

Figure 5.16 The airspeed distribution of the operator at the foot level 55
Figure 5.17 Position of the number 6 cross section 56
Figure 5.18 Temperature distribution of the operator in the chest position 56
Figure 5.19 The airspeed distribution of the operator in the chest position 57
Figure 5.20 Position of the number 7 cross section 58
Figure 5.21 Temperature distribution of the operator's in head position 58
Figure 5.22 Airspeed distribution of the operator's in head position 59
Figure 5.23 Temperature values of the operator at the foot level 61
Figure 5.24 Temperature distribution of the operator in the chest position 61
Figure 5.25 Temperature distribution of the operator's in head position 62

CHAPTER 1

INTRODUCTION

Before the 1990s, car design mostly steered to vehicle aerodynamic or motor studies than the thermal management of the driver compartment. Thermal comfort in vehicles was considered a luxury privilege. Over time, thermal comfort has become a more critical issue for customer satisfaction. In-car air conditioning modeling is essential not only for thermal comfort but also for safety [1]. Today, thermal comfort has become a more important criterion while choosing vehicles. An uncomfortable in-car environment may cause distraction and short or long periods of sleepiness of drivers. This uncomfortable environment could jeopardize driving safety.

Today's earthmoving machinery is equipped with cabs, and thermal comfort comes into prominence. One of the crucial factors that negatively affect the working conditions of operators in the earthmoving machinery is the ambient temperature. Due to the working conditions, operators can stand in the cabin for long hours. This situation affects the health of the operator negatively and reduces the capacity to work efficiently. In order to provide the maximum field of view in the cabins and prevent potential hazards, the glazed area of the driver's cab takes up quite a lot of space. This condition increases the uncertainty of heat exchange. Namely, since weather conditions are variable, to ensure pleasant air conditioning environment in the driver's cabs is a challenging process. Due to such reasons, the car air conditioning modeling, which will be carried out during the cabin design of the machine, can produce real results. As a result, airflow distribution performance in the driver's cab can be estimated, and optimization studies can be easily repeated before the air conditioning model is placed in the cab. System optimization studies are essential in different aspects. For example, the parameters within the vehicle such as the number of, the location of, design of the air vents can be changed in the modeling and the cost of experimental testings' which is done trying can be reduced. The design, which provides the best condition for the system, can be completed in a shorter time, saving

both cost and time. Besides, the air conditioning load requirement of a vehicle is determined, and air conditioning optimization studies are performed depending on the desired load.

1.1 Draft of the Thesis

In this thesis, a thermal distribution model and air flow pattern has been examined, including radiation effects in a machinery driver's cab. According to ISO 10263-4 standard, the points specified around the driver have been verified with the test results performed in the climatic test chamber [2]. The flow chart of the thesis is as follows,

In the first chapter, general information has been given in the introduction and literature studies on in-car air conditioning have been examined.

In the second chapter, the basics of the theoretical background used in the analysis of the numerical model have been explained.

In the third chapter, numerical model development in the thesis study has been examined.

In the fourth chapter, how to done climatic test chamber conditions has been expressed in detail.

In the fifth chapter, the results of the analysis of the numerical model have been interpreted, and the numerical model has been verified according to the results of the test.

In the sixth chapter, the conclusions of the thesis have been evaluated. Besides, ideas about future studies have been given to improve the analysis.

1.2 Purpose of the Thesis

In this thesis, air flow distribution and thermal distribution effects in a machinery driver’s cab have been investigated. For this process, a simplified flow model needs to use. It is also crucial that parameters, such as the solution methods used and

convergence criteria, are correctly given as inputs to the analysis. The purpose of this study is to create a numerical analysis model which is validated by test results. The verified numerical analysis model will be developed by adding new parameters for future studies.

1.3 Literature Review

1.3.1 Overview

When the literature studies are examined, it is seen that the studies of creating in-car air conditioning/ventilation modeling have been developed with the advancement of computer technology. Especially in the literature, air conditioning numerical flow analyses can be found for cars, trucks, airplanes, and railway wagons. In this section, a summary of essential literature sources related to thesis and used as a resource has been given.

1.3.2 Previous Studies

Shah et al. (2008) examined the thermal distribution and flow distribution analysis for the Volvo sleeper cab truck and the Mack truck [3]. Power consumption utilized by the HVAC system has a direct influence on the fuel economy of the truck, so the energy used by the Heating, Ventilation, Air Conditioner system is an important parameter to be considered in fuel economy. The heating and cooling models they prepared were solved numerically in the Fluent and RadTherm package programs. According to the data obtained, optimization studies were carried out on factors affecting air conditioning loads, such as insulation and material thickness. The amount of power required to operate the air conditioner at the desired efficiency was also reduced. Accordingly, the amount of fuel consumed for the air conditioner was also decreased. As a result, fuel economy was achieved by finding and optimizing the detection of vehicle air conditioning load.

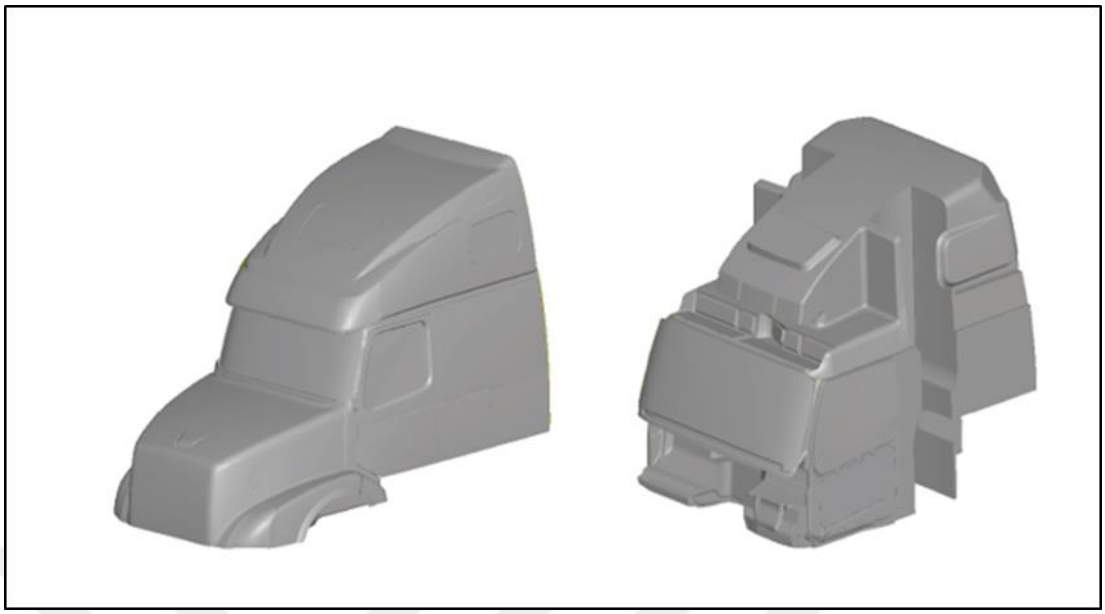

Figure 1.1 Surface geometry and CFD model surface geometry

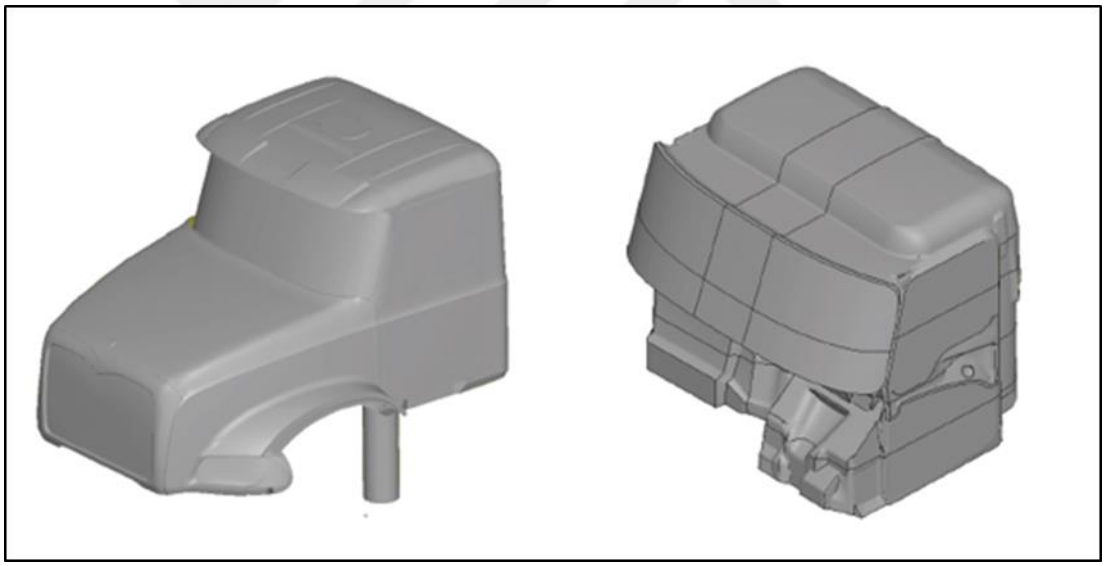

Figure 1.2 Surface geometry and CFD model surface geometry

Figure 1.1 and *Figure 1.2* show the Volvo sleeper cab truck and the Mack truck are surface geometry and CFD modeling, respectively [3].

Aronson et al. (2000) investigated the air-flow distribution in the car using the ventilation method [4]. Measurements had been made with particle image velocimetry

(PIV) in the vehicle to compare the air distribution of the numerical model obtained by air distribution of the vents in the vehicle. The results of the measurement and numerical model were found to be very close to each other.

Roy et al. (2001) explained the mechanisms of heat transfer on a geometrically and physically simplified model on their study [1]. They used the zonal approach method for this analysis. Zonal approach method disintegrates the physical space about the automotive car cabin an ensemble of simple geometric shapes, therefore decreasing many of the difficulties of generating a single grid about a complex shape, e.g., ensuring sufficient grid refinement near all body surfaces to capture the boundary layer. Information is propagated between zones via grid overlapping and a spatial interpolation procedure [5]. Thanks to this model approach, the solution of flow analysis was obtained in a shorter time. They published the results of thermal distribution within the car cabin on their study.

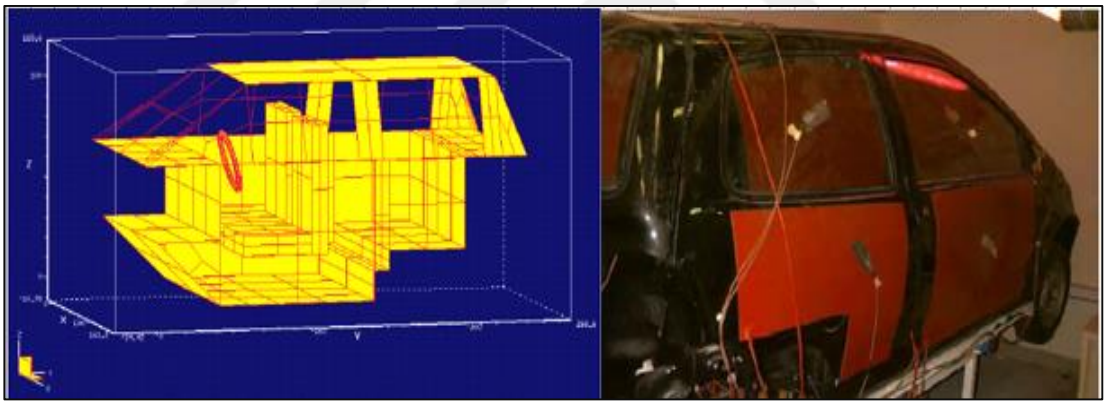

Figure 1.3 3D simplified picture of the car cabin and vehicle test bench

Figure 1.3 shows a 3D simplified representation of the car cabin and vehicle test bench, respectively [1].

Wang et al. (1991) examined the air-flow and contaminant concentration in a passenger cabin via the air-flow program PHOENICS [6]. According to the results of the analysis, it was done sixteen different studies by changing the position of air outlets and inlets. It was aimed to change the orientation of the air in the passenger cabin.

Also, it was taken into consideration occurred condensation on the surface of car glass. The best result was that the air outlets were located close to the sources of pollution. It was also emphasized that air outlets, which are a well-known principle in indoor climate technologies, should be positioned as close to pollution sources as possible. These sources of pollution can be smokers, heat sources, passengers, solar heat transmitted through windows.

Danca et al. (2016) performed work to evaluate a simple approach of calibrating and validating a CFD model that regenerate the thermal environment and the flow dynamics, inside a vehicular cabin [7]. This study was only a small part of a project that aims to evaluate different cabin ventilation strategies from the point of thermal comfort. Experimental data were compared with local comfort indices for air velocities and temperatures. The test results of the real vehicle and the numerical results of CFD modeling had been very compatible with each other, besides the effect of several parameters on the in-cabin environment has been examined numerically.

Alexandrov et al. (2001) investigated the importance of HVAC configuration in-cabin [8]. For example, the air temperatures and velocities at the inlets, the size number, and location of the system's inlets and outlets. Besides, the influence of external parameters such as outside temperature and vehicle speed on the climatic conditions in the car were also researched. The results were stated that the internal parameters, such as air velocities and temperatures at the inlet and outlet, as well as external parameters such as both car velocity and outside temperature, play an essential role in determining the efficiency of the car HVAC system. Another significant result was that the optimization of air inlets and outlets. Thanks to this optimization process, low air circulation zones inside the cabin were also improved.

Liu Hongmin analyzed the results of an air-conditioned ship's thermal environment by Airpak software [9]. A simulation model was prepared, and results were validated for this analysis. It was shown in the article that thermal comfort could be improved to some extent by air feed outlet and air return outlet, air feed temperature, and air feed rate modification. Low air conditioning system had been the best performing system.

The indoor air temperature of the low air conditioning system was 2 ~ 4 lower than the original air conditioning system and the two modified systems. Thus, it was concluded that the air feed temperature could be increased to a higher value to provide both thermal luxury and energy savings.

Axelsson et al. (1999) published in their articles that CFD could be provided comparable sensitivity to the experimental test of air distribution systems when both numerical and experimental methods are validated [10]. The air conditioning unit was thought to consist of two different parts. These were the air distribution system and passenger compartment. In the study, the air distribution system was analyzed in two different situations. These were ventilation and defroster conditions. In the ventilation analysis, the results were consistent with the test results, but there were differences in the defroster analysis. The reason for this situation was not fully understood. For future studies, they state that they will examine the geometric explanations of narrow cover openings, the effects of grid thinning and turbulence models on the flow distribution.

Chronéer et al. (1991) used the computational fluid dynamics to examine the flow distribution in the Volvo S80 driver's cab [11]. One of the essential reasons for this work was to create a safe CFD model that could be used in the development of an air conditioning system in the car in the future. Besides, they performed the mesh resolution study. For this study, from 1 million to 5 million different numbers of mesh size were studied, and the results were compared. Another important point mentioned in the article was where there was air leakage in the vehicle. In this study, it was also stated that inside vehicle air leaks significantly affected air flow distribution. Therefore, it was essential to understand where the leakage was and to create the right flow area to reduce the leakage as much as possible.

Currle et al. (2000) used the flow modeling of a Mercedes E-series car [12]. They made changes in the size of the side and middle air vents of the flow model. It was seen that the optimization studies on the dimensions of the air vents affected the air flow distribution within the cabin. These variables were taken as reference, and the air

distribution in the vehicle was examined in detail. They examined the changes in thermal comfort in the vehicle and published them in their articles.

Mohammad Aliahmadipour et al. (2017) expressed that in this study, numeric flow analysis was carried out to monitor the air flow characteristics of the air conditioning system in a passenger compartment in two different cases for summer conditions [13]. The test results were also contrasted with the numerical analysis, and a validation study was conducted. The results indicated that the position of the inlet air duct in the cabinet is essential for the air flow input from the HVAC system. The air is most inclined towards the left side of the room. Therefore, the air flow has deviated from the thermal comfort conditions in some parts of the cabinet. The results also show that some small changes to the partition design can improve HVAC system performance. Another result of this study is also that symmetrical air distribution creates the most suitable thermal comfort for the cabin.

Akdemir et al. (2016) examined the flow and temperature distribution in a tractor cab considering summer conditions [14]. Computational flow dynamics method was used for temperature and airflow analysis. Ansys Fluent program was utilized to observe the distribution of ambient conditions. Convection and radiation boundary conditions were defined on the flow modeling. Airflow and temperature distribution were shown in detail by taking the contours. Data of test measurements were taken at some points in the cabin for this analysis. Measurement results and analysis results were compared with the help of tables and graphs. According to the results, while the average temperature difference between the measurement and the model is 3.5 ℃, the average air velocity difference is 0.3 m/s.

Akdemir et al. (2012) used the CFD method to study the temperature and humidity distribution in a test room [15]. The primary purpose of the study was to keep agricultural products longer than they can withstand. Geometric and physical modeling was discussed in detail. The results of the CFD analysis were compared with experimental results step by step. According to the results obtained, they observed the effect of the placement of products in the room on the temperature and humidity

distribution. According to the results obtained from the analysis, optimization studies were carried out on cold storage. They published the results of temperature and velocity distribution within a test room as taking contours. In addition to all these results, it was indicated that the use of computational fluid dynamics is a potent source for better monitoring and understanding of any process within any environment.

Aroussi et al. (2003) conducted a numerical analysis to examine the icing or misting that occurred in a vehicle windscreen [16]. They also were examined the turbulent air-flow on the windshield of the vehicle. It was stated that the computational fluid dynamics method was applied successfully for air flow and heat transfer analysis. A good fit between the numerical results and the test results were achieved. Another result was that due to vehicle design, air flow velocities vary in the cab. This condition could cause some adverse effects in terms of driving comfort. It was studied thermal distribution in the cabin with the ANSYS Fluent program in detail.

Melih Akyol, in his study, interior comfort parameters of the cabin, which has an ever-changing and uneven distribution in the heating and cooling processes of automobiles, investigated [17]. These parameters are the amount of carbon dioxide in different outdoor conditions, different grate openings, and velocity level selections. The measurement results were compared with the prepared Matlab-Simulink model.

Conceição et al. (1999) examined the heat transfer balance and mechanisms in vehicle passenger compartments [18]. In the study conducted on railway wagons, the effects of solar rays in the cabin were investigated numerically and experimentally. The windows, ceilings, and internal temperatures of the train were defined under the conditions of the moving and stationary state of the train. They published their results by comparing the test results and the numerical model results.

CHAPTER 2

THEORETICAL BACKGROUND

2.1 Overview

In this section, a plot summary of the theory and approaches utilized in this thesis have been explained. K-epsilon realizable turbulence model, solar radiation, the governing equations of fluid mechanics and the models utilized in FLUENT's version R1 are expressed shortly.

2.2 Fluid Dynamics

Fluid mechanics is the science that examines the physical behavior of substances called fluids, and it deals with the interaction of fluids with solids or other fluids at the boundaries. Fluid mechanics itself is split into several categories. Applicable, work on the movement of incompressible fluids (e.g., liquids, especially water and low-speed gases) is generally called hydrodynamic. A hydrodynamic sub-category is hydraulic that deals with fluid flow in pipes and open channels. The gas dynamics is related to the flow of liquids that pass important density variations, such as the flow of gases at high speeds through the nozzles. The aerodynamic category interests in the gas flow (mainly air) at high or low speeds in objects such as aircraft, rocket, and automobile [19].

Navier Stokes equations are used as governing equations in fluid dynamics [20]. These equations justify that the momentum changes affecting the unit mass in the fluid are equal to the sum of the viscous forces that cause pressure changes and friction losses. These viscous forces consist of intermolecular interactions and show how resistant the fluid is against to flow. Thus, it can be said that the Navier-Stokes equations are a dynamic expression of the balance of forces in any region of the given fluid. Some assumptions are made in these equations; for example, the fluid is considered to be a continuous flow. So, the fluid flow is considered to be the same form everywhere.

These equations are derived from physical principles conservation of mass, conservation of momentum, and conservation of energy. The three conservation laws are utilized to untie fluid dynamics problems, and the mathematical formulation takes into consideration the concept of a control volume (CV).

The control volume used in fluid dynamics and thermodynamics is a mathematical abstraction. It is used to create mathematical modeling of a physical process. It is a volume fixed in space or moving with constant velocity through which the fluid flows. The control surface is called the surface surrounding the surface of the control volume. [21].

2.2.1 Conservation of Mass

The conservation of mass relation for a closed system changing is denoted as

m_{sys} = constant or $\frac{dm_{sys}}{dt} = 0$, the mass of the system does not change throughout a process.

Conservation of mass is defined as follows,

Conservation of mass: $\dot{m}_{in} - \dot{m}_{out} = \frac{dm_{cv}}{dt}$ **(2.1)**

$\dot{m}_{in}$ total rate mass flow into control volume, $\dot{m}_{out}$ total rate mass flow out control volume, dm_{cv}/dt is the rate of change of mass within control volume boundaries [19].

Mass continuity, the conservation of mass, which states that the rate of alteration inside a control volume must be equal to the net rate of fluid flow into the volume [22].

$$\frac{\partial}{\partial t} \iiint_V \rho dV = - \iint_S \rho \mathbf{u} \cdot \mathbf{dS} \quad \textbf{(2.2)}$$

ρ is the fluid density, u is a velocity vector and t is time. The differential form of the continuity equation is, by the divergence theorem:

$$\frac{\partial \rho}{\partial t} + \nabla \cdot (\rho \mathbf{u}) = 0 \quad \textbf{(2.3)}$$

For steady flow,

$$\partial/\partial t = 0 \quad \textbf{(2.4)}$$

$$\oiint \rho \, \mathbf{u} \cdot \mathbf{dS} = 0 \quad \textbf{(2.5)}$$

$$\nabla \cdot (\rho \mathbf{u}) = 0 \quad \textbf{(2.6)}$$

Incompressible flows: $\frac{d\rho}{dt} = \vec{\nabla} \cdot \vec{\mathbf{u}} = 0 \ (\text{constant density})$ **(2.7)**

2.2.2 Conservation of Momentum

The conservation of momentum, the forces acting on the control volume consist of the mass forces (such as gravity, electric and magnetic forces) acting on the whole mass of the control volume and the surface forces (such as pressure and shear stress acting on the control surface forces) acting on the control surface. Newton's second law of motion, applied to a control volume, states that any change in the momentum of the fluid in that control volume originates from the effect of the net momentum flow in the volume and the external forces affecting on the liquid. [19].

Newton's second law,

$$\frac{d}{dt}(m\vec{v}) = \vec{\mathbf{F}} \quad \textbf{(2.8)}$$

applied to fluid flow is, Equation (3.7) is the momentum equation in integral form.

$$\frac{\partial}{\partial t} \iiint_V \rho u dV = - \oiint_S (\rho u \cdot dS) u - \oiint_S p \cdot dS + \iiint_V \rho \mathbf{f_{body}} dV + F_{viscous} \quad \textbf{(2.9)}$$

The equations shown below are partial differential equations that correlate the flow field properties of momentum at the x, y and z components, respectively.

$$\frac{\partial (\rho u)}{\partial t} + \nabla\cdot(\rho u \boldsymbol{V}) = -\frac{\partial p}{\partial x} + \rho f_x + (F_x)_{viscous} \quad \textbf{(2.10)}$$

$$\frac{\partial (\rho v)}{\partial t} + \nabla \cdot (\rho v \mathbf{V}) = -\frac{\partial p}{\partial y} + \rho f_y + (F_y)_{viscous} \quad \textbf{(2.11)}$$

$$\frac{\partial (\rho w)}{\partial t} + \nabla\cdot(\rho w \mathbf{V}) = -\frac{\partial p}{\partial z} + \rho f_z + (F_z)_{viscous} \quad \textbf{(2.12)}$$

where the subscripts x, y, and z on f and F denote y and z components of the body and viscous forces, respectively. The above equations are used for the unsteady state of the three-dimensional flow of any fluid. This flow may be viscous or inviscid and may be compressible or incompressible properties [22].

2.2.3 Conservation of Energy

Although energy can be converted from one form to another, the total energy in a closed system always remains constant. The energy equation is as follows,

$$\rho \frac{Dh}{Dt} = \frac{Dp}{Dt} + \nabla\cdot(k\nabla T) + \Phi \quad \textbf{(2.13)}$$

h is enthalpy, k is thermal conductivity of the fluid, T is temperature and ϕ is the viscous dissipation function. The statement on the left side is a material derivative [23].

2.3 Buoyancy Model

Because of the temperature alterations occurring in a convective flow, it causes some changes in the distinctive properties of the liquid, which makes the understanding of the analysis very complicated, so some approaches must be used. In the Boussinesq approach, differences of all fluid properties apart from density are entirely ignored, as well as density variations are disregarded as long as they create a gravitational force [24].

Buoyancy currents occur as a result of the change in the density of the fluid, also that it can also define as currents that can change position by gaining momentum due to

factors such as gravity and centrifugal forces. If this current is only due to the temperature difference, it is called natural convection. The warm fluid will have a lower density than the cold fluid and then be ascendant in the opposite direction to gravity. This behavior can be expressed as follows:

$$u\frac{\partial u}{\partial x}+v\frac{\partial u}{\partial x}=-\frac{g}{\rho}(\rho_{\infty}-\rho)+\frac{\mu}{\rho}\frac{\partial^2 u}{\rho\partial y^2} \quad \textbf{(2.14)}$$

where the first term on the right side is the buoyancy force induced by the density variation, the equation above is derived through assuming a steady, 2-D, for incompressible flow with regular features excluding density change due to the buoyancy forces.

As mentioned earlier, the change in density is caused by temperature change. Therefore, equations need to add a temperature term. This term is β. It is a measure of how much the density alters with the change in temperature at constant pressure. In this case:

$$\beta=-\frac{1}{\rho}\frac{\partial p}{\partial T}\Big/\approx-\frac{1}{\rho}\frac{\rho_{\infty}-\rho}{T_{\infty}-T} \quad \textbf{(2.15)}$$

$$(\rho_{\infty}-\rho)g\approx-\rho_0\beta(T-T_{\infty})g \quad \textbf{(2.16)}$$

In this case, the momentum equation in the direction of gravity,

$$u\frac{\partial u}{\partial x}+v\frac{\partial u}{\partial x}=-g\beta(T-T_{\infty})+\frac{\mu}{\rho}\frac{\partial^2}{\rho\partial y^2} \quad \textbf{(2.17)}$$

It is the inverse of β, total temperature for ideal gases. It can be defined as below:

$$\rho=\frac{p}{RT} \quad \textbf{(2.18)}$$

$$\beta=\frac{1}{\rho}\frac{\rho}{RT^2}=\frac{1}{T} \quad \textbf{(2.19)}$$

2.4 Types of Heat Transfer Mechanisms

In a medium or between the mediums, in all cases where there is a temperature difference, the heat transfer occurs. In general, heat transfer can be defined as the transfer of heat between two or more different objects through conduction, convection, and radiation.

2.4.1 Heat Conduction

Conduction heat transfer can be considered as the transfer of energy from higher energy particles of a substance to lower energy particles as a result of interactions between these particles. It is possible to examine the heat transfer process with the appropriate time rate of equations, and these equations can be used to calculate the energy transmitted per unit time. The law of heat conduction is also as Fourier's law and a one-dimensional flat wall for Fourier's law is expressed as follows:

$$q''_x = -k\frac{dT}{dx} \tag{2.20}$$

where q''_x is heat flux (W/m^2), k is the coefficient of thermal conductivity (W/m.K), d The same formula is valid for the structures that it is called a mixed wall consisting of several steps, but for this, the equivalent heat transfer coefficient needs to find. For this reason, an equivalent thermal resistance (R) is found, and solutions are made as using this thermal contact resistance for the compound walls. The layers of such walls may comprise a plurality of series and parallel thermal resistance as they are comprised of different materials. For the wall with n layers' parallel to each other:

$$q_x = \frac{T_{\infty,1} - T_{\infty,n}}{\sum R} \tag{2.21}$$

It is also possible to work with the heat transfer coefficient U, which is defined similarly to the Newtonian cooling law in mixed systems. The equation for this approach is as follows:

$$q_x \equiv UA\Delta T \tag{2.22}$$

ΔT is the total temperature difference.

The total heat transfer coefficient calculation for compound walls is shown below:

$$U = \frac{1}{R_{total} A} = \frac{1}{[(1/h_1)+(L_1/k_1)+\ldots(1/h_n)+(L_n/k_n)]} \quad \textbf{(2.23)}$$

Generally,

$$R_{total} = \sum R_t = \frac{\Delta T}{q} = \frac{1}{UA} \quad \textbf{(2.24)}$$

2.4.2 Heat Convection

The heat transmission due to the temperature difference between the fluid in motion and its surrounding surface is called convection heat transfer. The following equation defines it:

$$q'' = h(T_s - T_\infty) \quad \textbf{(2.25)}$$

In this formula h convection heat transfer coefficient, T_s is surface temperatıre and T_∞ is the temperature of the fluid.

The convection heat transfer coefficient can be calculated according to the flow theory on a two-dimensional flat surface. The convection heat transfer coefficient is described below as a function of the number of Prandtl (Pr).

$$Nu = \frac{hL}{k} = 0.664\, Re^{0.5} * Pr^{1/3} \quad \textbf{(2.26)}$$

$$Re = \frac{\rho v L}{\mu} = \frac{vL}{\nu} \quad \textbf{(2.27)}$$

Pr is Prandtl number; Re is Reynolds number, Nu is Nusselt number, k is the plate's coefficient of heat conduction, L is the surface length, ν is kinematic viscosity of the fluid, μ is molecular viscosity of the fluid and v refers to the flow rate on the surface.

2.4.3 Radiation

Thermal radiation is the energy emitted by an object that is temperature different from zero. The energy of the radiation field is transmitted by electromagnetic waves (or photons). While transmission of energy by conduction or convection requires the existence of a material environment, this is not necessary for radiation.

The radiation emitted by the surface originates from the thermal energy of the object surrounding the surface and the energy released from the unit surface at the unit time is emissivity power is called the E (W/m^2).

$$E_b = \sigma T_s^{\,4} \tag{2.28}$$

In the above equation, T_s is absolute temperature (K), σ is Stefan-Boltzmann constant ($\sigma = 5.67\times10^{-8}$ $W/m^2 \cdot K^4$). Such a surface is called the ideal radiation emitter or black surface.

The heat flux emitted by a truth surface is less than an emitted by a black body at the same temperature, and is given by the following equation:

$$E = \epsilon\, \sigma T_s^{\,4} \tag{2.29}$$

In this equation, ε is called the emissivity rate and is about radiation property of the surface, and shows a value in the range $0 < \epsilon < 1$. It shows how much a surface radiates energy compared to a black body.

Radiation may occur from several sources such as the sun or other surfaces in the visual field of the surface in question. Regardless of the sources, all of this radiation coming to the unit area of the surface per unit time is called the incoming radiation G.

The surface may absorb some or all of the incoming radiation, and therefore, an increase in the thermal energy of the material occurs. The radiation energy absorbed per unit time in the unit area of the surface can be calculated if the absorption rate α,

which is a radiation property of the surface, is known. This property value in the range $0 < \alpha < 1$, and is defined as,

$$G_{abs} = \alpha G \quad \textbf{(2.30)}$$

If the surface is radio-opaque $\alpha < 1$ a part of incident radiation is reflected. If the surface is semi-permeable, some of the incident rays pass, some of it is absorbed, and the rest is reflected. In this case,

$$\alpha + \rho + \tau = 1 \quad \textbf{(2.31)}$$

in the above equation, α is absorption radiation ratio, ρ is reflected radiation ratio, τ is transmitted radiation ratio.

2.5 COMPUTATIONAL FLUID DYNAMICS (CFD)

Computational fluid dynamics is a fluid mechanics science that uses numerical methods and algorithms to analyze and solve fluid mechanics problems. The basic equations governing fluid motion describe as the Navier-Stokes equation. Fluid (gas and liquid) solves with the aid of partial differential equations representing the conservation laws for mass, momentum, and energy [25]. The equations can be simplified by looking at what effects can be neglected.

There are several critical dimensionless numbers used in fluid dynamics. Dimensionless numbers are significant for understanding the importance of various effects and for identifying the characteristics of the fluid flow. These are dimensionless numbers like Reynolds number, Mach number, and Nusselt number [26].

- Reynolds Number

Reynolds number gives information about the characteristic of the fluid. Namely, gives information about whether fluid flow is turbulent. It indicates the ratio of inertia forces to viscous forces.

$$\mathrm{Re} = \frac{\rho UL}{\mu} \quad \textbf{(2.32)}$$

where ρ is a density of the fluid (kg/m^3), L is the characteristic length of the geometry (m), U is the velocity of the fluid (m/s), μ is the dynamic viscosity of the fluid (Pa·s or N·s / m^2)

- Mach Number

Mach number is the local flow-speed, V, divided by the sound of speed in the a.

$$M = \frac{V}{a} \quad \textbf{(2.33)}$$

- Nusselt Number

It is only the ratio of convective heat transfer to conductive heat transfer.

$$Nu_L = \frac{hL}{k_f} \quad \textbf{(2.34)}$$

where h is the convective heat transfer coefficient of the flow, L is the characteristic length, k is the thermal conductivity of the fluid.

- Prandtl Number

The ratio of momentum diffusivity to thermal diffusivity.

$$Pr = \frac{\nu}{\alpha} \quad \textbf{(2.35)}$$

ν is momentum diffusivity, α is thermal diffusivity.

2.6 Turbulence

Fluid flow split into two main categories: laminar flow and turbulent flow. Turbulent flow is time-dependent and is challenging to identify without using numerical methods due to the high fluctuations of the fluid. It is quite challenging to solve the governing

equations used in fluid dynamics without using simplifications and approaches. Using these simplifications and approximations processes helps us solve the problem that needs to be solved both more accurately and with fewer errors. Besides, there are some numerical methods used to solve 3D Navier-Stokes equations directly. These equations define as Direct Numerical Simulation. This direct solution method uses in the desired analysis where the error function is minimal. Nevertheless, these numerical approaches are ineffectively time-wasting and subsequently not utilized in the industrial analysis.

One of the simplifications methods is Reynolds Averaging approach. In the Reynolds averaging, the variables sudden in the Navier-Stokes equations separate into one fluctuating and one averaged parts. For the velocity components:

$$u_i = \bar{u}_i + u'_i \tag{2.36}$$

where $\bar{u}_i$ and u'_i are the mean and fluctuating velocity components.

Alike, for pressure and other scalar quantities,

$$\zeta = \bar{\zeta} + \zeta' \tag{2.37}$$

where ζ denotes a scalar, e.g., pressure, energy, or species concentration.

Placing statements of this form for the flow variables into the instant continuity and momentum equations and taking a time average produces the ensemble-averaging momentum equations. As a result, the Reynolds averaged Navier-Stokes (RANS) equations are obtained and are written as:

$$\frac{\partial \rho}{\partial t} + \frac{\partial}{\partial x_i}(\rho u_i) = 0 \tag{2.38}$$

$$\frac{\partial}{\partial t}(\rho u_i) + \frac{\partial}{\partial x_j}(\rho u_i u_j) = -\frac{\partial p}{\partial x_i} + \frac{\partial}{\partial x_j}\left[\mu\left(\frac{\partial u_i}{\partial x_j} + \frac{\partial u_j}{\partial x_i} - \frac{2}{3}\delta_{ij}\frac{\partial u_l}{\partial x_l}\right)\right] + \frac{\partial}{\partial x_j}(-\rho\overline{u_i' u_j'}) \tag{2.39}$$

where $\overline{u_i' u_j'}$ is Reynolds stress tensor. It explains the relationship between the velocity of turbulent's flows. Boussinesq hypothesis can be used to solve this stress tensor [27].

2.7 K-epsilon Realizable

K-epsilon Realizable viscous model has been used for this thesis. The k-epsilon turbulence models are robust and rather detailed for many non-boundaries governed flows and thus recommended. It is also ideal in terms of solution time. K, which is the turbulence kinetic energy, and ε, which is the rate of dissipation, are defined for continuous and incompressible flows as follows:

$$\frac{\partial}{\partial t}(\rho k) + \frac{\partial}{\partial x_j}(\rho k u_j) = \frac{\partial}{\partial x_j}\left[\left(\mu + \frac{\mu_t}{\sigma_k}\right)\frac{\partial k}{\partial x_j}\right] + G_k + G_b - \rho\varepsilon - Y_m + S_k \quad \textbf{(2.40)}$$

$$\frac{\partial}{\partial t}\rho\varepsilon + \frac{\partial}{\partial x_j}(\rho\varepsilon u_j) = \frac{\partial}{\partial x_j}\left[\left(\mu + \frac{\mu_t}{\sigma_\varepsilon}\right)\frac{\partial \varepsilon}{\partial x_j}\right] + \rho C_1 S\varepsilon + \rho C_2 \frac{\varepsilon^2}{k+\sqrt{v\varepsilon}} + C_{1\varepsilon}\frac{\varepsilon}{k}C_{3\varepsilon}P_b + S_\varepsilon \quad \textbf{(2.41)}$$

$$C_1 = max[0.43\frac{\eta}{\eta+5}] \quad \textbf{(2.42)}$$

$$\eta = S\frac{k}{\varepsilon} \quad \textbf{(2.43)}$$

$$S = \sqrt{2S_{ij}S_{ij}} \quad \textbf{(2.44)}$$

In the equations, G_k is a degree of the creation of the turbulence kinetic energy from the mean velocity gradients, G_b is the produced turbulence kinetic energy because of buoyancy and Y_M signifies the influence of the fluctuating dilatation incompressible turbulence to the general propagation rate and is significant for High-Mach-number flows. C_1 and $C_{1\varepsilon}$ are constants and σ_k accompanied by σ_ε are turbulent Prandtl numbers for k and ε, S_k and S_ε are user-defined source terms, respectively.

The fixed numbers used for this model are given below;

$C_{1\varepsilon} = 1{,}44$, $C_2=1{,}9$, $\sigma_k=1$, $\sigma_\varepsilon=1{,}2$

2.8 Wall Functions

It is one of the critical and challenging issues for Computational Fluid Dynamics (CFD) where viscous effects become important and how to examine the thin near-wall sublayer. In the case of heat transfer, the correct solubility of this layer is significant, because the majority of the temperature change develops in it. The most reliable way is to use a fine grid and a low-Re-number model [28].

On the other hand, this is both a very time-consuming process, and most of the fluid flows are turbulent. So, the traditional industrial solution has been to use wall-functions. Wall functions are getting used to finding variables, for instance, velocity, turbulence, and pressure approximately in the region near a wall called the boundary layer. If wall functions are not used in the numerical analysis, it will be a complicated process to solve fluid behavior.

The velocity profile of the wall equations in the logarithmic field is as shown below:

$$u^+ = \frac{\overline{v_t}}{u_\tau} = \frac{1}{\kappa} ln(y^+) + B \qquad \textbf{(2.45)}$$

in the equations, u_t is shear velocity, κ is the Karman constant which is equal to 0.41, $\overline{v_t}$ is the mean velocity parallel to the wall, B an experimental derived constant about the thickness of the viscous sublayer, y^+ is the dimensionless distance from the wall [29].

$$u_\tau = \sqrt{|\tau_w|/\rho} \qquad \textbf{(2.46)}$$

τ_w is the shear stress at the wall.

$$y^+ = \frac{\rho u_\tau y}{\mu} \quad \textbf{(2.47)}$$

2.9 Solar Load Model

ANSYS FLUENT offers a solar load model to calculate the effects of radiation from the sun rays on computational models. In this thesis, the S2S radiation model, which is defined as surface to surface, was used as a solar load model together with the solar ray tracing algorithm. The solar ray tracing method is a beneficial and practical method for applying solar energy loads as heat sources in the energy equations, and S2S radiation model can be used to regard the radiation alteration in an environing of gray-diffuse surfaces. The energy change between the two surfaces for the S2S model counts relatively on the size, orientation and separation distance of the surfaces and these parameters are calculated by a geometric function so-called a 'view factor'. The S2S radiation model base upon the calculation of a view factor file and this file contains data related to irradiative surfaces. The calculation of this file is a very resource-requiring and time-consuming process. To minimize the calculation time of the surfaces involved in the radiation it is necessary to minimize the number of surfaces. The surface-to-surface (S2S) radiation model is well for modeling the radiative enclosure transfer without participating environment, but it has some limitations, and therefore when using the S2S radiation model, the following limitations should be paid attention:

- The S2S model supposes that all surfaces are diffuse and gray radiation.
- The S2S model with the hemicube view factor method cannot utilize if model involves symmetry or periodic boundary conditions in addition to that, it cannot be put to use as a model participating in radiation problems.
- The S2S model does not promote hanging node implementation on radiating boundary zones.

2.9.1 Solar Ray Tracing Algorithm

The Solar Ray Tracing algorithm makes use of a positioning vector for 'the solar location' also called sun direction vector and two illumination parameters to set the solar intensity. These properties are applied to any or all wall, porous jump, and inlet/outlet boundary zones, in short, all boundary conditions on the model. The Solar Ray Tracing algorithm calculates the heat flux on the boundary faces that stem from the incident radiation, and this heat flux is coupled to the ANSYS Fluent calculation by the use of a source term in the energy equation. The solar calculator is in needs of statements of the coordinates of where the model is its located or global position, time and date of day, mesh orientation, solar irradiation method and sunshine factor in computing the sun direction vector and the magnitudes of the illumination parameters.

There are two illumination parameters: direct solar irradiation and diffuse solar irradiation. Direct solar illumination utilizes the two-band spectral model to occur distinct material properties in the visible and infrared bands. The diffuse solar irradiation makes use of a single-band hemispherical-averaged spectral model.

Absorptivity and transmissivity values should be indicated for direct visible, direct IR, and diffuse hemispherical when applying the solar boundary conditions on the model. While defining a semi-transparent material needs a detailing of absorptivity and transmissivity, such as glass. However, when defining an opaque material, it is sufficient to define absorptivity only. Absorptivity and transmissivity parameters provide to adjust both right color boundary and correct properties, of the semi-transparent and opaque materials. Transmissivity and absorptivity values identified for normal incident rays, but ANSYS Fluent interpolates these values for the set angle of incidence. Solar ray tracing method should not use for non-conformal interfaces.

The shading calculation to involve the presence of shading that uses for solar ray tracing is an essential application of vector geometry. A method of reducing the ray tracing algorithm is applied to decrease the ray tracing algorithm complexity that can cause long run times for 10^4 faces and bigger. If the mesh is higher than five million

cells, a rise in this parameter will lessen the simulation time needed to calculate the solar loads.

The radiation emitted from the sun can be applied to several types of glass and plastic glass materials on the wall boundaries and to the effects of coated glazings modeled using solar ray tracing algorithm. To model solar's optical specifications, the transmissivity and reflectivity have to be specified in the wall boundary conditions. Glazing optical properties vary the incident angle, importantly for larger angles than 40.

2.9.2 Surface to Surface Radiation Model (S2S)

The radiation model comprises the radiation exchange in an enclosure of grey surface. According to ANSYS Fluent's S2S radiation model, surfaces are assumable to be gray and diffuse that emissivity and absorptivity properties of grey surfaces are independent of the incident wavelength, and also by Kirchoff's law, the emissivity equals the absorptivity [27].

Another assumption in S2S radiation model is that the exchange of irradiative energy (E) between surfaces is nearly uninfluenced by the medium that separates them; the energy incident on the surface is either reflected (ρE) or transmitted (τE) and a fraction (αE) is absorbed. As the surfaces are opaque to thermal radiation (in the infrared spectrum), the surfaces may be thought opaque.

$$\alpha + \rho = 1 \qquad \textbf{(2.48)}$$

since α is equal to the emissivity (ε), and $\rho = 1-\varepsilon$.

The energy equation utilized in the surface to surface model is consisting of directly emitted and reflected energy. The reflected energy flux is dependent on the energy incident on the surface and later can be expressed concerning the energy flux leaving all radiating surfaces. The energy leaving from the surface k is described as:

$$q_{out,k} = \varepsilon_k \sigma {T^4}_k + \rho_k q_{in,k} \quad \textbf{(2.49)}$$

$q_{out,k}$ the enrgy flux coming from the surface of k, $q_{in,k}$ the energy flux incident on the surface, ε_k is the emissivity constant, σ is the Boltzmann's constant, ρ_k is reflected energy constant and T is the temperature.

CHAPTER 3

NUMERICAL MODEL DEVELOPMENT

3.1 Overview

In this thesis, the methodology has been composed of two main parts. At first, the model development process has been explained, later model validation and results have been described. Much effort has been tried harder to understanding the use of the ANSYS FLUENT software and improving the numerical approach. Many academic sources have been examined for a literature search. Also, videos of flow and tutorials have been benefited from during the process of building the analysis model.

In this section, it discusses what to do need in the process of creating an analysis modeling. The numerical model development process has been set up in three subheadings.

- Firstly, the geometry of the model has been cleaned.
- Secondly, thermal calculations have been made.
- Finally, the model has been established in numerically, and boundary conditions have been determined.

3.2 Creation Process of Model Geometry

To create a numerical model and calculate in package software, the air flow volume of the model is required. This flow volume is one-piece, so all discrete parts in the model must be properly connected. 3D geometric data has been cleaned with the help of SPACE CLAIM software. Because the geometry is very complex and consists of dozens of different components, creating a flow modeling has taken a long time. Geometric details that cannot affect the flow field must be deleted before meshing. Because these details make it difficult for both the meshing process and extend the computational time. Surface mesh data has been created in ANSYS FLUENT Meshing

module of the prepared geometric data. As the errors occurred during the meshing process, it has been gotten back to the geometry, and the necessary corrections have been made. This process has been repeated many times. After the geometric data has been thoroughly cleaned at the desired level, the meshing process has been started. ANSYS Fluent meshing program is a very successful software to mesh complex geometries. First, the surface mesh is created in this program. Then it is corrected the imperfect zones and optimized the surface mesh quality as much as possible. According to the Fluent meshing guide, the surface mesh skewness value must be at most 0.7. The purpose of this condition is to ensure that the quality of the volume mesh is good. The better the volume mesh quality, the lower the convergence time of the analysis, and the more precise results.

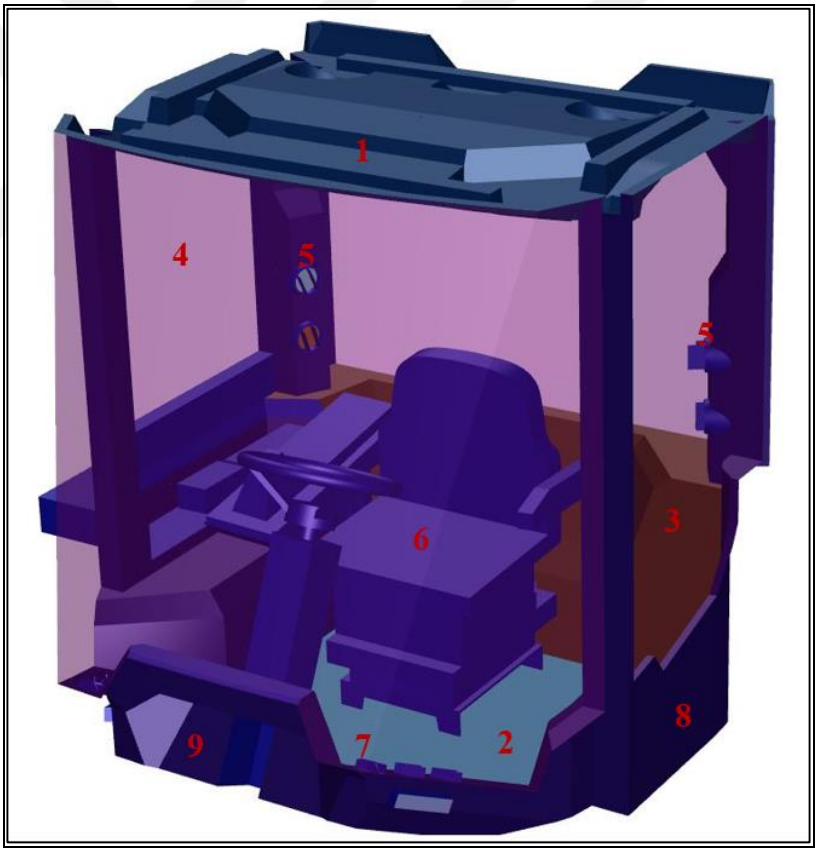

Figure 3.1 The model geometry used in simulations

Figure 3.1 shows the geometry of the modeled cabin. Name of the numbers on the model are respectively,

1- Ceiling, 2- Ground, 3- The cabin wall close to the engine, 4- Cab glass, 5- The air inlets at the rear of the cab, 6- The operator's seat and steering wheel, 7- The air inlets at the front of the cab, 8- Door tread plate, 9- Front plate.

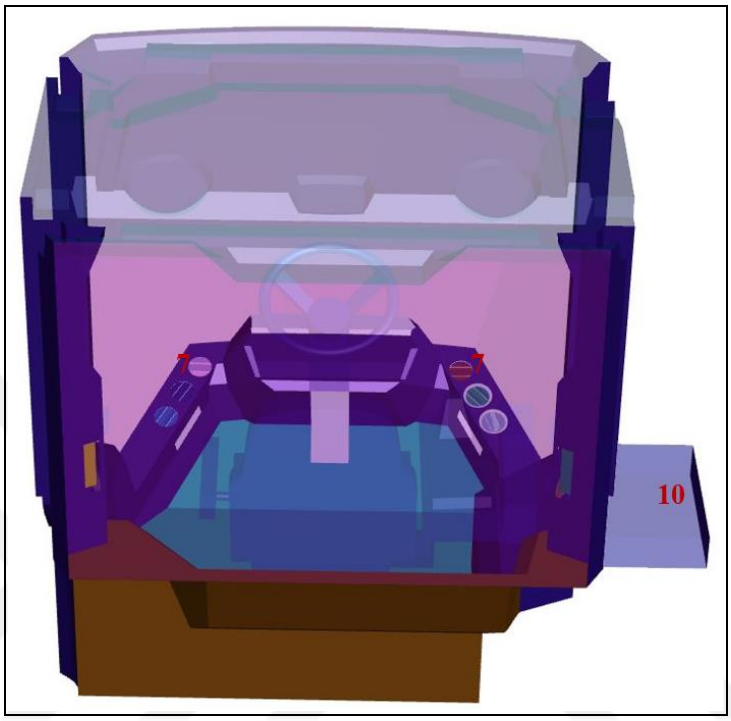

Figure 3.2 Detailed representation of air inlets in front of the cabin.

Figure 3.2 has shown a detailed shape of air inlets in front of the cabin. Besides, the number ten (10) represents the air outlet.

After the surface mesh process was completed, the creation of the volume mesh process has been started. The volume meshes have also been created ANSYS FLUENT Meshing program. A set of calculations have been carried out for different mesh sizes both to optimize computation times and to take mesh size independent results. So, the outcomes of mesh resolution and mesh size have been examined by changing the number of cells from 1 million to nearly 14.3 million. Four meshes have been made up with 1, 3, 6.9 and 14.3 million cells respectively.

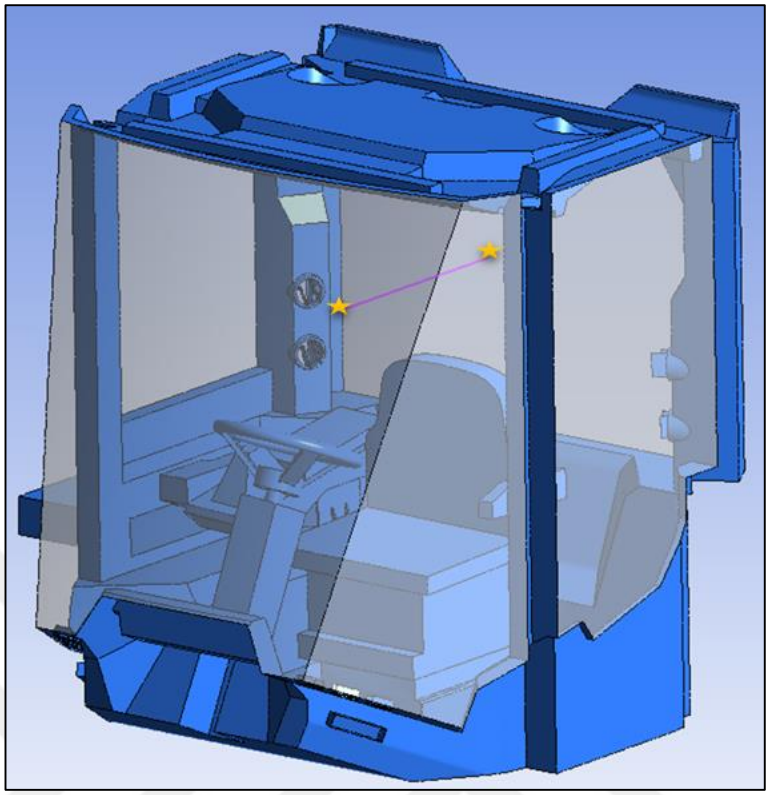

Figure 3.3 The position of the line in the cabin



Figure 3.4 Mesh independence study

Benchmarking must be required to able to decide which mesh size is sufficient for the solution. For comparison, a straight line has been drawn in the cabin, as shown in *Figure 3.3*. One hundred points have been defined on the line in the direction of the y component of the air velocity, and the velocity values have been read. For all mesh studies, this line has been used. *Figure 3.4* shows the results of mesh studies. According to results, between 6.9 million mesh and 14.9 million mesh studies, the results have been found to vary by a maximum of five percent. Namely, the number of mesh generated by more than 6.9 million has been no longer seen to affect the results.

Consequently, it has been found that as a minimum, 6.9 million cells are needed to a mesh independence study. 6.9 million mesh has been used for this thesis study, both in terms of taking accurate results and reducing computational time. The surface mesh had a maximum skewness value of 0.6, and the volume mesh had skewness value 0.9. Polyhedral mesh type has been used for volume mesh. Aspect Ratio has been used as the boundary layer method for analysis, and ten prism layers have been used for near –wall modeling.

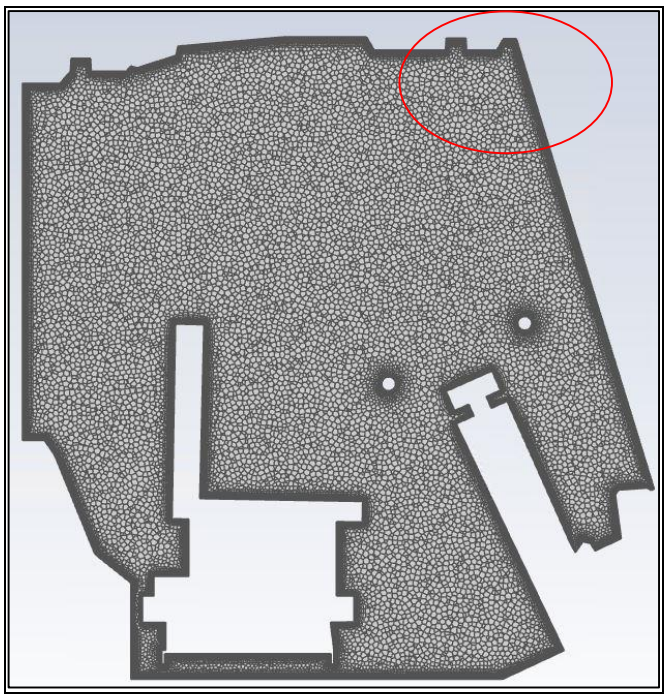

Figure 3.5 Detailed mesh view on the cross-section

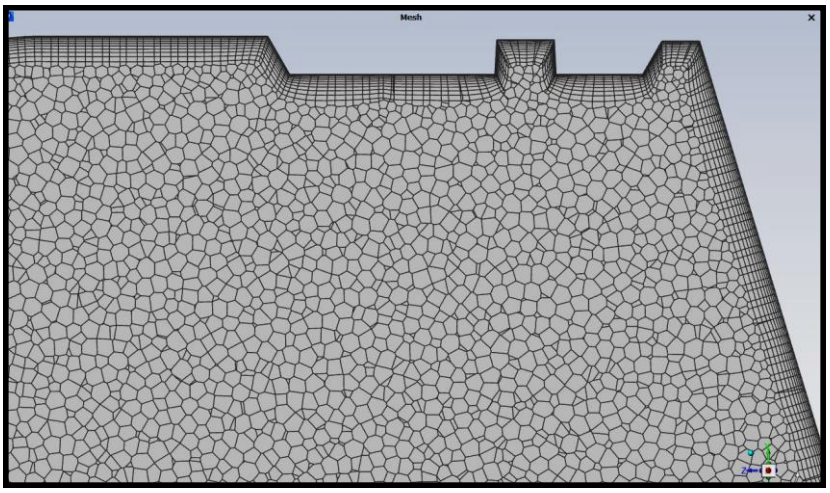

Figure 3.6 Inflation layer detailed representation

Figure 3.5 shows a detailed mesh view on the cross-section. Also, in *Figure 3.5*, the section taken inside the circle shows the inflation layer, and it is given *Figure 3.6* in detail. Figure *3.7* indicates the general view of the driver's cab mesh surfaces.

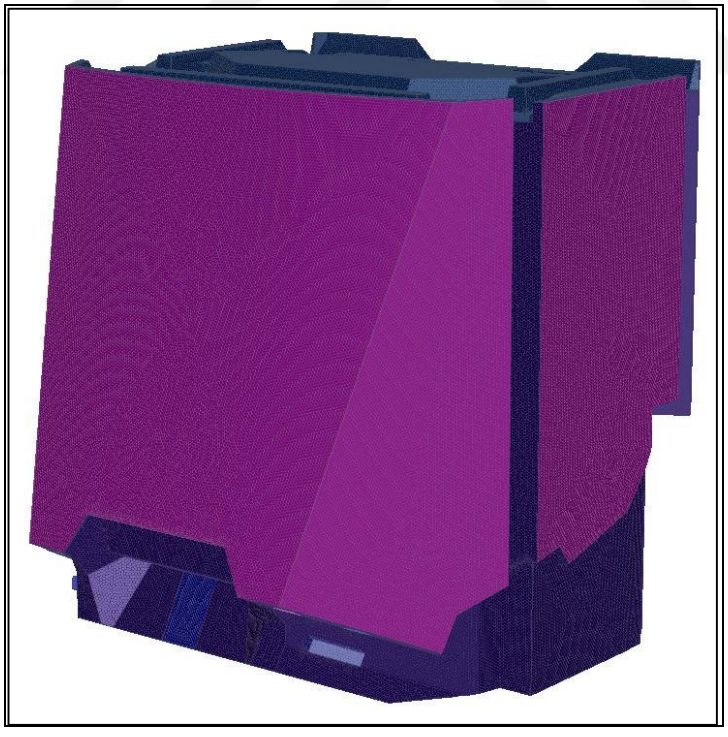

Figure 3.7 General view of the driver's cab mesh surfaces

3.3 Thermal Calculations

During the creation of the mathematical model, the effect of the conduction, convection, radiation, and various combinations of these (coupled) have been taken into consideration. In the developed mathematical model, the driver's cab has been simulated in testing condition. Therefore, the conduction heat transfer coefficients of the multi-layer wall portions separating the outside of the cab and the interior have been found.

As indicated in section 2.4.2, flow theory on a two-dimensional flat surface was used to add the effect of the air flow outside the cabin to the calculations. In this way, convection heat transfer coefficients have been calculated for the surfaces on-vehicle with an average running speed of 10 km/h (2,7 m/s). The total heat transfer coefficient of the multilayer walls between the inside and outside of the cabin must be determined to calculate the convection heat transfer coefficient. According to section 2.4.2, convection heat transfer coefficient outside the cabin 10 W/m^2K, inside the cabin 3 W/m^2K was done calculations by accepting.

It has not been made radiation calculations. The radiation module inside the ANSYS FLUENT program has been used. Details have been explained in section 3.4 Numerical Setup.

3.4 Numerical Setup

The numerical models examined has been set up in the ANSYS FLUENT R1 program. The mesh current in the development study composed of nearly 6.9 million polyhedral cells and has been created in ANSYS Fluent meshing.

The used solver settings as follows:

- Segregated solver (Pressure based solver)
- Steady state condition
- K-epsilon turbulence model
- Enhanced wall treatment-thermal effects for near-wall modeling

- Energy model
- Surface to Surface (S2S) radiation model (Activated for the second analysis)
- Solar ray tracing (Activated for the second analysis)
- Body-Force weighted velocity coupling
- Boussinesq approximation for including buoyancy

The discretization method for all simulations has been for energy a second order scheme and for solving of momentum a second order upwind. The data collected during the air-conditioner test has been used as boundary conditions in the numerical model. These data have been the velocity and temperature values in the vehicle air inlets. Test conditions have been explained in detail in CHAPTER 4. The convergence criteria for the model were 1E-4 for continuity, 1E-4 for momentum equations, and 1E-7 for energy. Buoyancy effect has also been included in the energy equation, using a Boussinesq approximation, to catch the main points the effects of rising hot air and sinking cold air. Incompressible ideal-gas has been used for air density for this analysis.

The air inlets have been steered to the machine operator and the windows, and the air inlets have been defined as inlet conditions. So that, different air mass fluxes, inlet velocities, inlet temperature or inflow directions as well as vent areas, etc. may be adjusted very readily.

Three different thermal boundary conditions have been used to solve energy equations. These are convection, temperature, and mixed heat transfer types. The boundary conditions of the cabin wall and glasses show the thermal characteristic of the materials of which are made, while the boundary conditions for the seat and steering have been accepted to adiabatic.

The convection boundary condition enables examining the effects of air flow outside the vehicle on the heat transfer mechanism of the vehicle. Calculations conducted in section 3.3 have been defined as the boundary condition into the solver program.

Typically, if identification is not made for the walls in the ANSYS Fluent program by the user, the walls are considered as zero thickness. In this case, there is no thermal resistance against heat transfer. When the thickness is defined for the walls, there are some cases where conduction is significant not only as a normal direction but also in the planar directions. There are different alternatives to provide this situation. One of them is the shell conduction option under the convection boundary condition. In this thesis, the shell conduction approach has been used. According to this approach, layers of wall cells are kept away from the fluid zone, and layers are enumerated sequentially, and prism layers are formed starting from the closest surface to the wall. Thanks to this approach, the thickness and conductivity features of each layer are easily defined [27].

During the air conditioning tests, temperature values have been taken from the wall surface close to the engine compartment, and for this wall, the average of these values has been given as the temperature boundary condition.

Firstly, cabin air conditioning tests have been performed in a controlled climatic test chamber. Therefore, for the first analysis, the conditions of the climatic test chamber have been simulated. In this analysis, a validated CFD model has been found out by comparing the data obtained from the air conditioning test and the results obtained from numerical modeling. A second analysis has been performed using the CFD modeling, which has been verified by the results of the air conditioning test performed in the climatic test chamber. The purpose of this analysis was to examine as a numerically the state of the machine in the real operating conditions. Solar radiation effects have also been included in this analysis. By incorporating solar radiation, the impact of solar radiation on the cab has been investigated. The amount of solar radiation acting on the driver's cabin has been given directly to the ANSYS Fluent program.

Two essential parameters adjust solar representation. These are direct solar irradiation and diffuse solar irradiation. While direct solar illumination calculates the visible and infrared bands radiations, diffuse solar irradiation calculates hemispherical averaged

spectrum. For all simulations, the value of direct solar irradiation value has been defined as 1100 W/m^2. The value of diffuse irradiation value has been defined as 250 W/m^2. Constant direction vector in FLUENT has been used to adjusting the solar position. Direction vector coordinates was set up [0,866, -0.5]. In *Figure 3.8* was shown the solar direction vector.

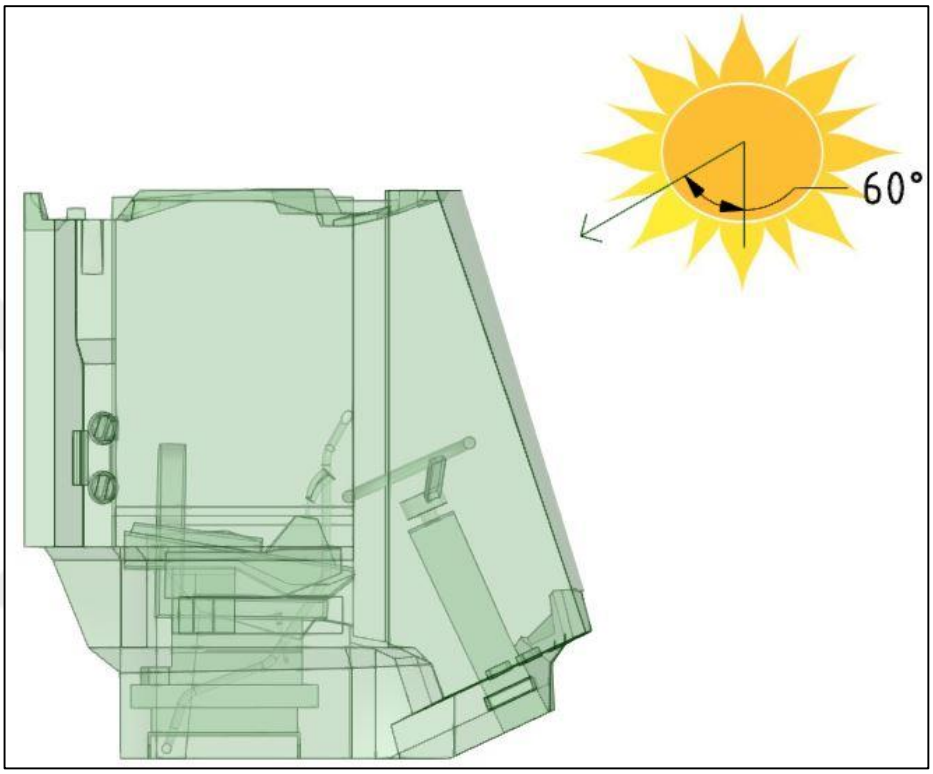

Figure 3.8 Representation of the solar direction vector

Models in the Fluent R1 version, it has been resolved in about four days in 11000 steps (iteration) on a supercomputer with 256 GB ram and 12 CPU using parallel processing option and double precision option.

Air inlet points have been enumerated as in *Figure 3.9* and *Figure 3.10*.



Figure 3.9 Numbering order of fore air inlets

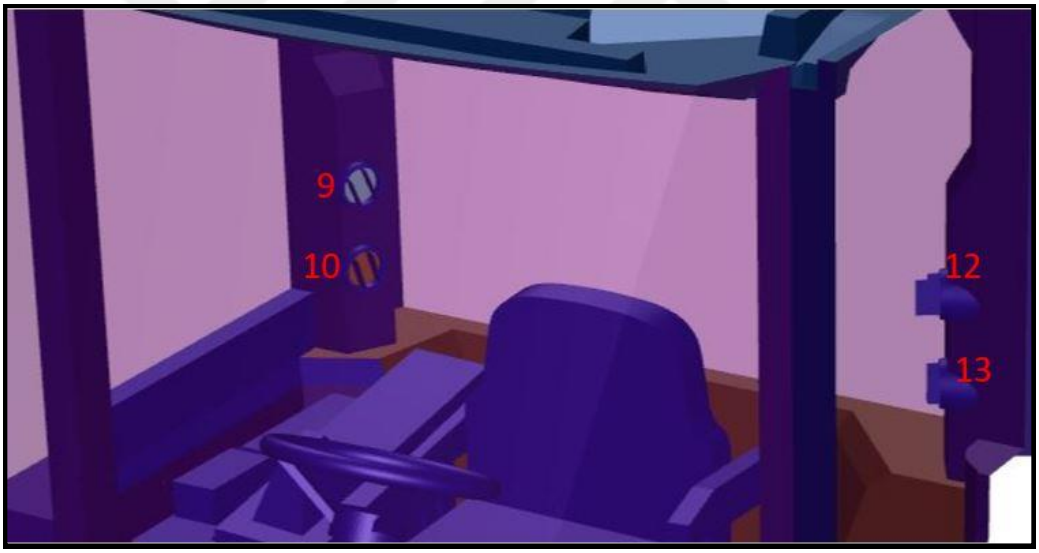

Figure 3.10 Order of numbering of the air inlets located in the back

According to the data obtained from the climatic test chamber results, the average velocity and temperature values of the air inlets used in the first analysis have been denoted in *Table 3.1*.

Table 3.1 Average velocity and temperature values of air inlets for the first analysis

Air Inlets	Velocity (m/s)	Temperature (K)	Temperature (°C)
1	3.7	284	11
2	4	283.9	10.7
3	4.5	283.8	10.6
4	2.3	283.7	10.4
5	3.2	281	7.6
6	2.6	280.1	6.9
7	2.2	280.4	7.2
8	2.1	281	7.4
9	5.8	285	11.4
10	6	284	10.8
11	5	283	9.8
12	5.3	282.8	9.6
13	6	282	8.5
14	4.1	281.4	8.2

According to the data obtained from the real working environment test results, the average velocity and temperature values of the air inlets used in the second analysis have been denoted in *Table 3.2*.

Table 3.2 Average velocity and temperature values of air inlets for second analysis

Air Inlets	Velocity (m/s)	Temperature (K)	Temperature (°C)
1	4	283	10
2	4.3	283.7	10.5
3	4.8	283.8	10.6
4	2.5	283.3	10.1
5	3	280.5	7.3
6	2.8	280.1	6.9
7	2	280	6.85
8	2.1	280.6	7.1
9	6	284.4	11.2
10	6.3	283.8	10.6
11	5	280	6.8
12	5.8	282.6	9.4
13	6.5	281.4	8.2
14	4.7	281.9	8.7

CHAPTER 4

TEST CONDITIONS

4.1 Overview

In this section, the test conditions of the driver’s cab explained, and types of test equipment used are mentioned. The driver’s cab cooling test is done according to ISO 10263-4 standard [2].

4.2 Test Conditions of Driver's Cab

The test conditions for the first analysis are as follows;

- The machinery driver’s cab has been tested in a climatic test chamber.
- The climatic test chamber is conditioned at a temperature of 45 degrees.
- The doors of the vehicle in the climatic test chamber are fully open before the test starts, to ensure that the indoor cabin air and external environment are in the same conditions.
- After the test begins, the doors of the driver's cab are closed, and the air conditioning is adjusted according to the cooling condition at maximum operating speed.
- There is no operator in the driver's cab during the test.
- There are fourteen air inlets and one air outlet in the driver's cab.
- According to the seat index points defined by ISO 5353, temperature measurements have been taken from at specific locations around the operator. In addition to these points, temperature and velocity measurements have been taken from the air inlets.
- The average of the data collected during the air-conditioner test has been used as boundary conditions in the numerical model, and these data are the velocity and temperature values in the cab air inlets.

- Since the test has been carried out under these conditions, the created numerical model has been simulated in this situation.

The test conditions for the second analysis are as follows;

- The machinery driver's cab has been tested in real operating working conditions.
- The machinery has been subject to solar radiation for three hours.
- The indoor ambient temperature has reached approximately 45 degrees.
- Solar radiation measurement has been done with the help of pyranometer.
- The air conditioning is adjusted according to the cooling condition at maximum operating speed.
- There is no operator in the driver's cab during the test.
- There are fourteen air inlets and one air outlet in the driver's cab.
- According to the seat index points defined by ISO 5353, temperature measurements have been taken from at specific locations around the operator. In addition to these points, temperature and velocity measurements have been taken from the air inlets.
- The average of the data collected during the test has been used as boundary conditions in the numerical model, and these data are the velocity and temperature values in the cab air inlets.
- Since the test has been carried out under these conditions, the created numerical model has been simulated in this situation.

4.3 Test Equipment

4.3.1 Air Flow Meters

Directional hotwire probe and Vane probe with thermocouple have been used for air velocity measurements. *Figure 4.1* is given airflow meters image.

- AP471S1 - Directional hotwire probe

Directional hotwire probe to measure air-speed in the range 0.1...40m/s and air temperature in the range -25°C...+80°C [30].

- AP 472S1 – Vane probe with thermocouple

Vane probe with K type thermocouple ∅ 100 mm to measure air-speed in the range 0.6…25m/s and air temperature in the range –25°C…+80°C [31].



Figure 4.1 Airflow meters

4.3.2 Type K Thermocouple

Type K Thermocouple has been used for temperature measurements. K Type is the most common type of thermocouple, as well as cheap, accurate, and reliable. It has a wide range of temperatures. The type K is commonly found in nuclear applications due to relative radiation rigidity. Thermocouple grade wire, –454 to 2,300F (–270 to 1260C), Extension wire, 32 to 392F (0 to 200C) [32].

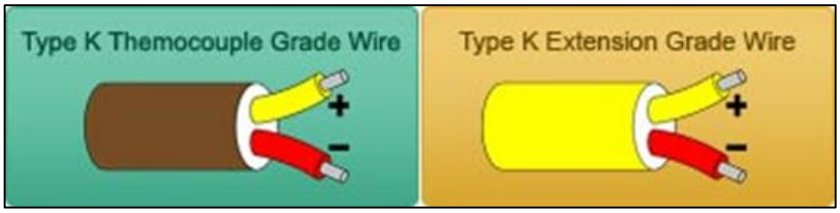

Figure 4.2 Type K Thermocouple [32]

4.3.3 Pyranometer

There are different types of pyranometers. One of them is thermopile pyranometer. A thermopile pyranometer is the "true" pyranometer that gauges the total amount of radiation on a surface utilizing a thermopile detector, a device that turns thermal energy into electrical energy. A thermopile pyranometer has a horizontal surface covered with a light absorbent black coloring that uses up radiation from the sun. A temperature difference occurs between the black surface and the body of the device, causing in a small voltage measured in watts per square meter. In this thesis, the type of pyranometer used as a solar radiation measurement instrument is a first-class thermopile pyranometer according to the ISO 9060 standard. Its model is LP PYRA 02 AV and measuring range is 0-2000 W/m^2. A semiconductor pyranometer measures radiation using a photodiode, a device that turns light into a current. An electrical signal is generated from the solar radiation absorbed. Semiconductor pyranometers are usually less reliable than thermopile pyranometers. Because it cannot catch the sun's entire spectrum, and it gives an error in measurements [33]. *Figure 4.3* has been given a pyranometer image.



Figure 4.3 Pyranometer [33]

CHAPTER 5

RESULTS of NUMERICAL MODEL

5.1 Overview

In this section, verification of numerical analyzes has been done. Besides, sections have been taken from inside of the cabin, and the temperature and velocity distributions have been investigated locally.

5.2 Verification Process Steps

5.2.1 First analysis: Climatic Test Chamber

For this thesis study, fifty different modeling's have been studied concerning both geometry modeling and identified the boundary conditions. The differences between modeling's had been scrutinized, and the modeling closest to the test results have been shown in detail this section. According to the seat index points defined by ISO 5353, temperature measurements have been taken from at specific locations around the operator. In *Figure 5.1* has been shown the position of the points. The model validation process has been done comparing with the data collected during the test, as stated in the previous sections. The numerical model created runs at a steady state condition for all simulations. For this reason, the average values of the points specified for the verify operation have been taken. Two conditions for test study must be taken into account, according to ISO 10263-4 standard [2]. Firstly, the temperature changes between point 2 and point 5 shall not more than 5 ℃, in *Figure 5.1*. Secondly, the maximum wind speed passing the machine from front to rear is 5 m/s. The measurement point locations have taken during the test are approximately has been entered in at the numerical analysis. The interval of error measurement of thermocouples used is ±3 degrees. For these reasons, the ± 3 ℃ temperature difference between experimental results and CFD results is determined as an acceptable condition in model verification. Verification studies have been conducted only by comparing temperature values while the

distribution of airspeed inside of the cabin has been interpreted according to the results obtained from the numerical analysis.

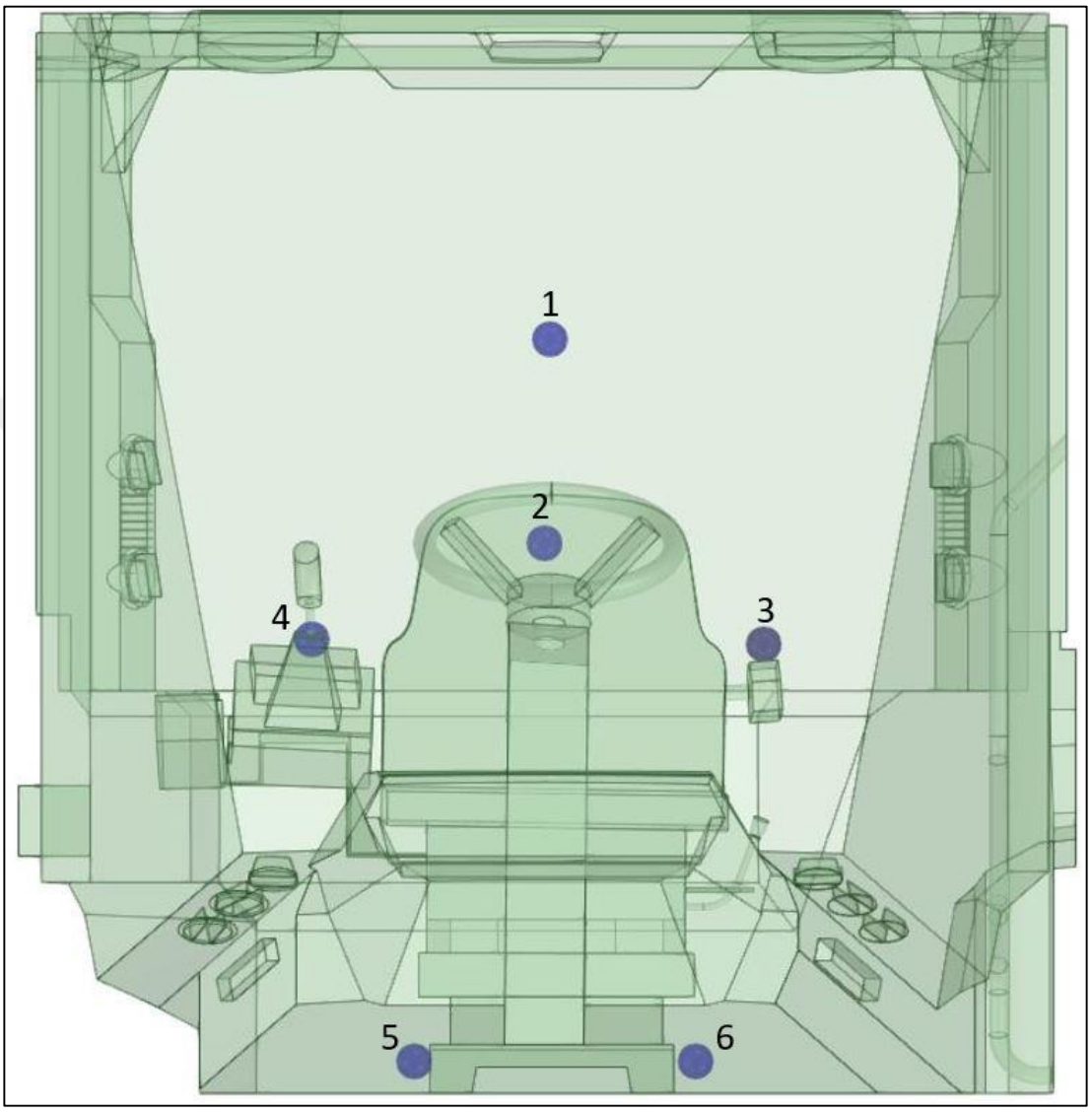

Figure 5.1 Measurement point locations

1: Head Position, 2: Steering position, 3: Right arm position, 4: Left arm position, 5: Right foot position, 6: Left foot position.

Table 5.1 Differences between temperature measurement and analysis results for the first analysis

Points	Average temperature experimental results (K)	Average temperature CFD results (K)	Difference (°C)
Head position	293.15	294.2	1.05
Steering position	295.65	296.8	1.15
Right-arm position	295.4	294.3	1.1
Left-arm position	294.3	293.8	0.5
Right-foot position	291	292.1	1.1
Left-foot position	292.75	291.55	1.2

Table 5.1, the average results of the CFD and the experimental have been compared. According to the results, it has been seen that the results of the CFD and the results of the test have been very close to each other at the desired points. The model accuracy has been accepted by providing the temperature difference condition.

In the following figures, cross sections have been taken in different locations in order to be able to observe in detail the temperature and velocity distributions in the machinery driver's cab. Results were taken from the ANSYS CFD-POST program.

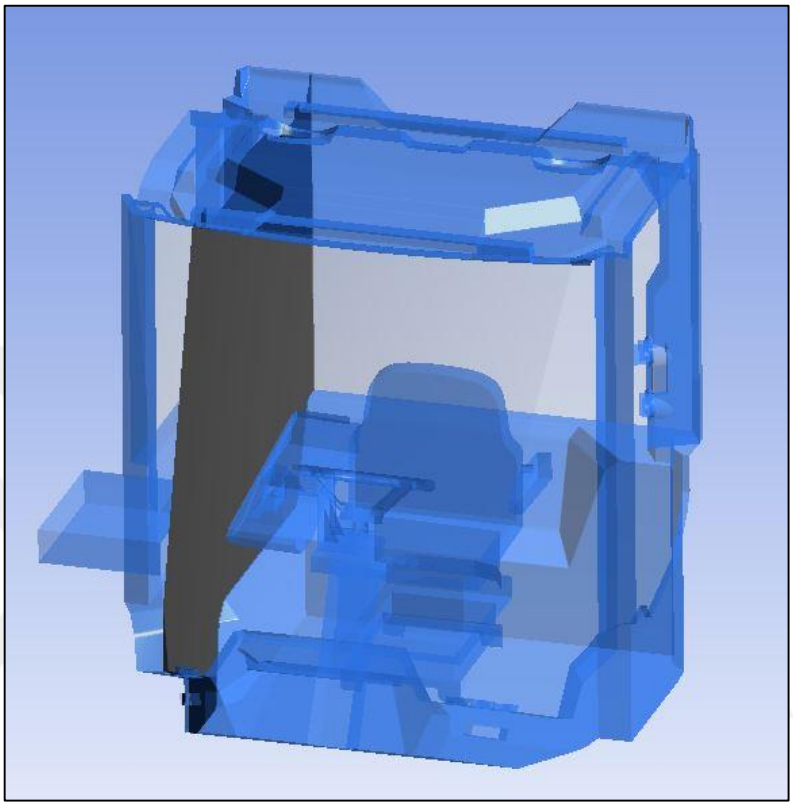

Figure 5.2 Position of the number 1 cross section

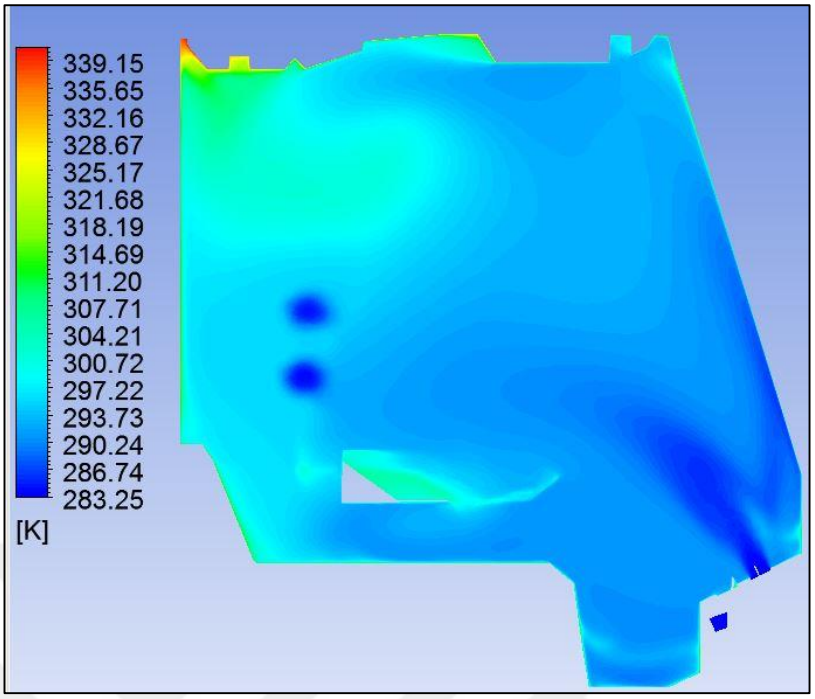

Figure 5.3 The temperature distribution of number 1 cross section

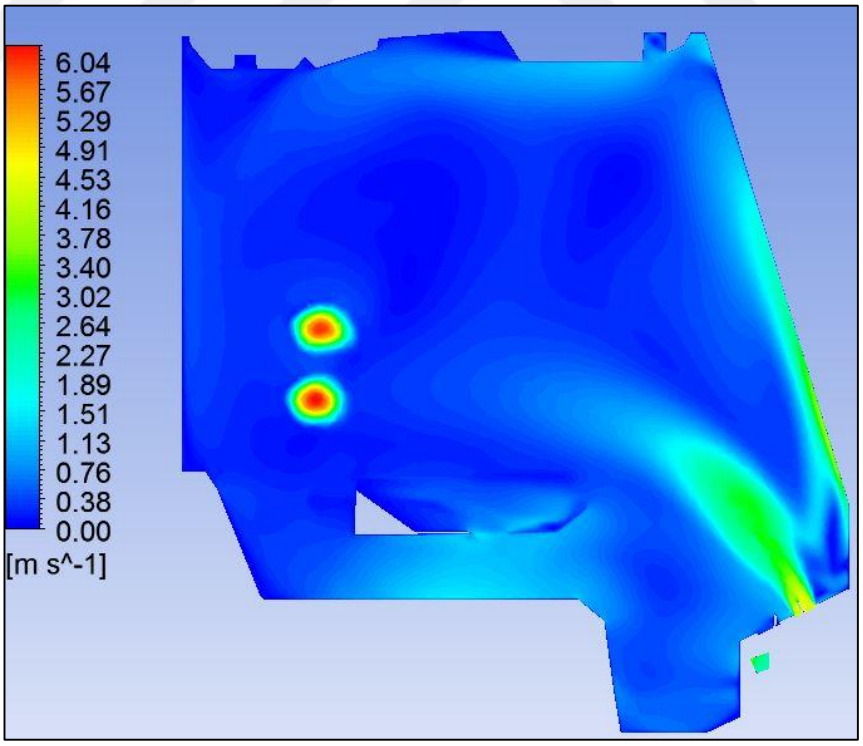

Figure 5.4 The airspeed distribution of number 1 cross section

Figure 5.2 shows the location of number 1 cross-section. *Figure 5.3* demonstrates the different temperature values of the number one cross-section between 10-41 °C. *Figure 5.4* illustrates the airspeed changes on a plane. Since the cross-section is taken over the air inlet point, the airspeed values in these parts are seen to be high.

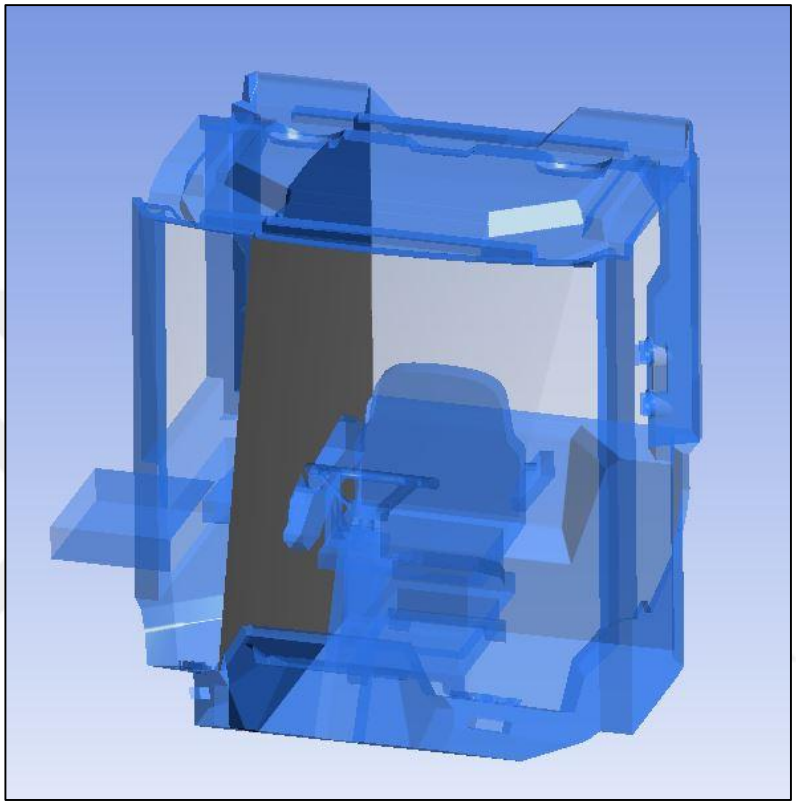

Figure 5.5 Position of the number 2 cross section

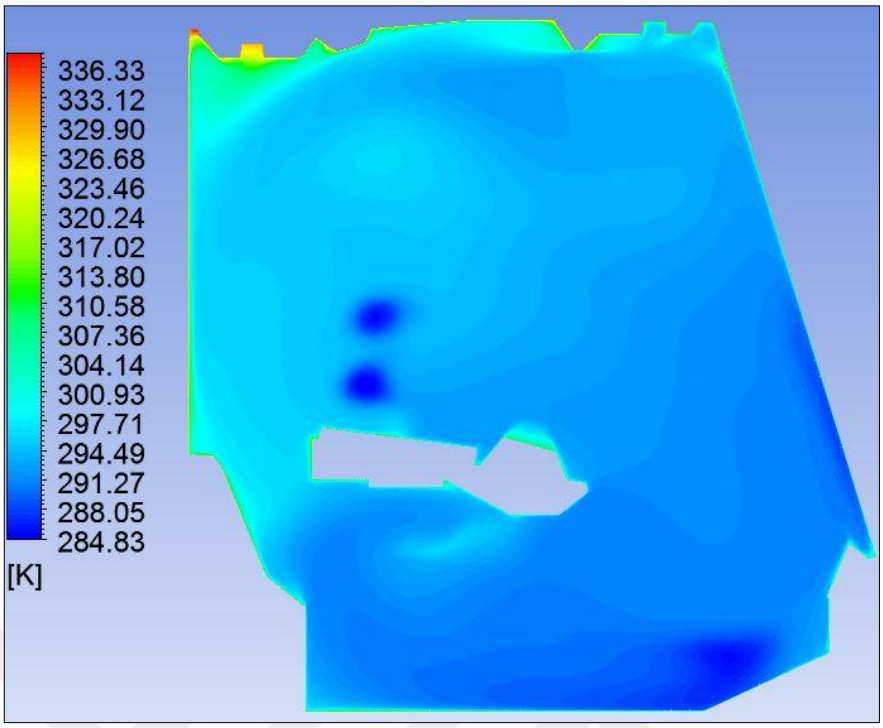

Figure 5.6 The temperature distribution of number 2 cross section

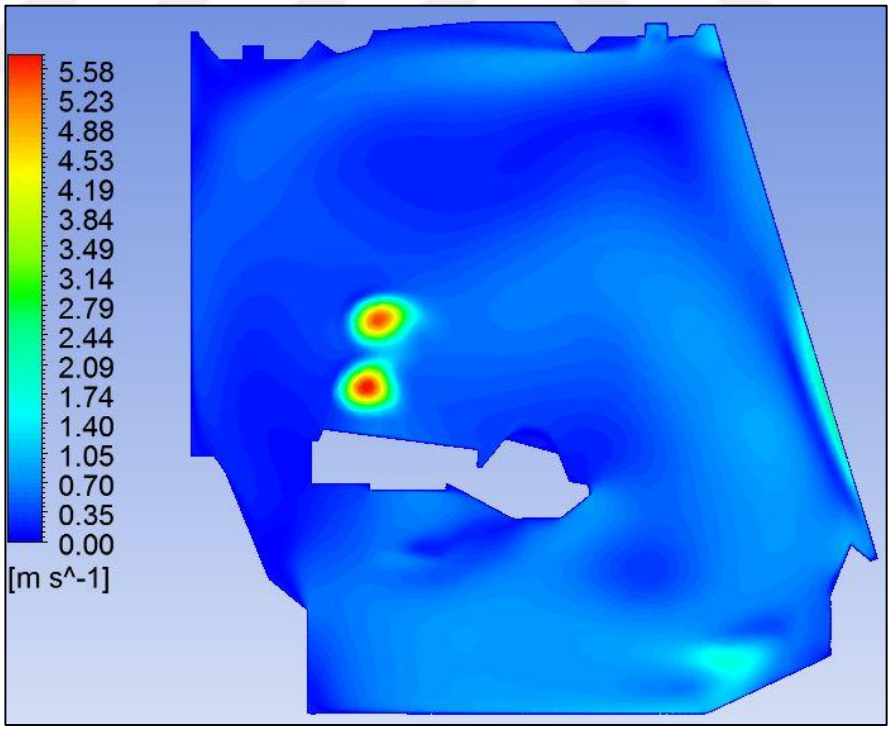

Figure 5.7 The airspeed distribution of number 2 cross section

Figure 5.5 shows the location of number 2 cross-section. *Figure 5.6* demonstrates the different temperature values of the number 2 cross-section between 11-48 °C. *Figure 5.7* illustrates the airspeed changes on a plane. When the cross-section is examined, the air velocity values are high in places close to the air inlet, but in other areas, it is around 1 m/s on average.

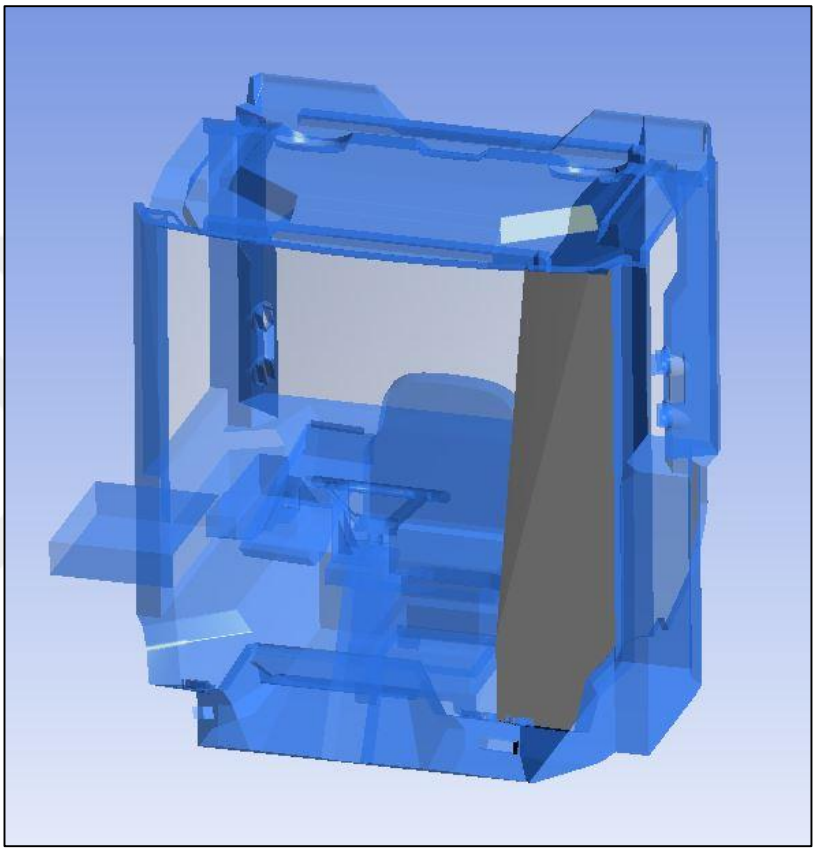

Figure 5.8 Position of the number 3 cross section

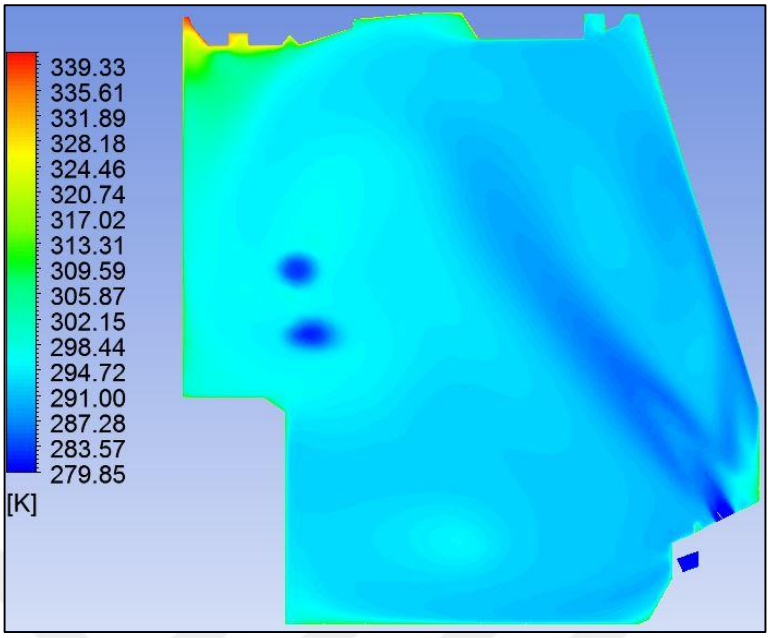

Figure 5.9 The temperature distribution of number 3 cross section

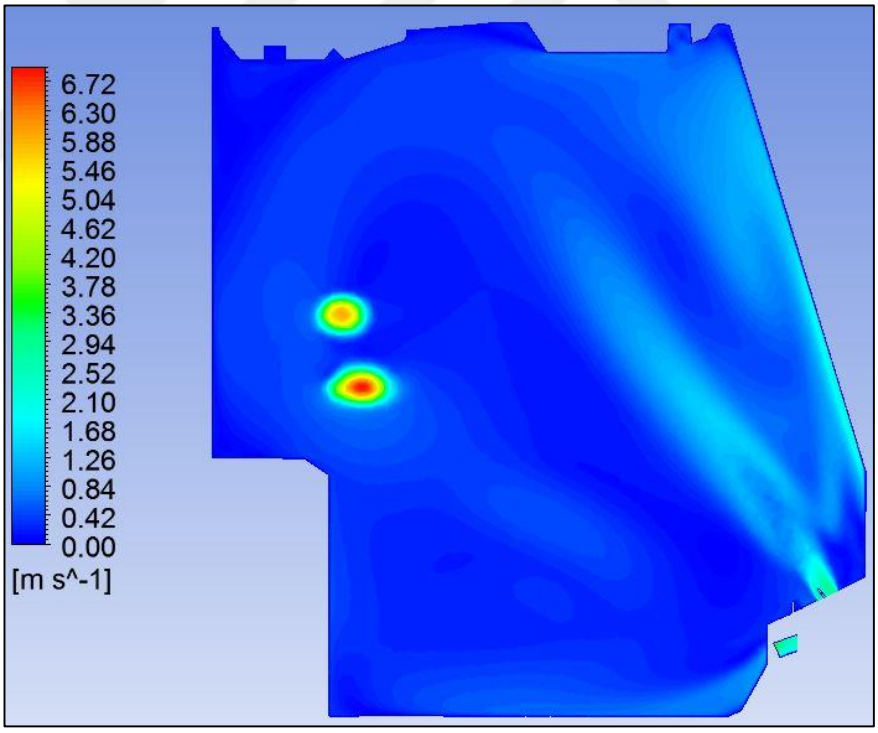

Figure 5.10 The airspeed distribution of number 3 cross section

Figure 5.8 demonstrates the location of number 3 cross-section. *Figure 5.9* shows the different temperature values of the number 3 cross-section between 6.5-37 °C. *Figure*

5.10 illustrates the airspeed distributions on a plane. It has been observed that both air velocity values and temperature values on this plane were lower than number 1 cross section.

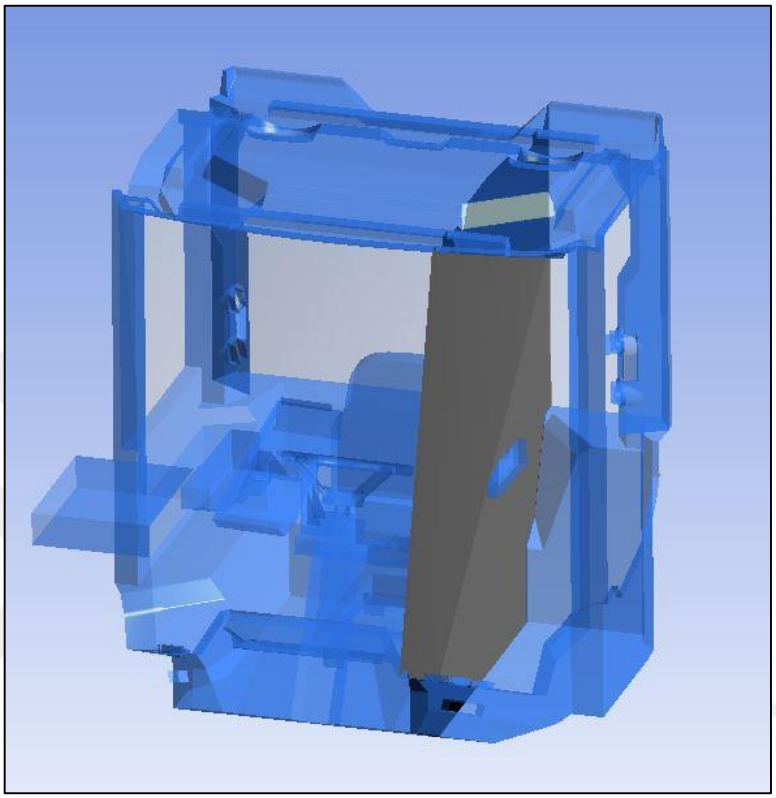

Figure 5.11 Position of the number 4 cross section

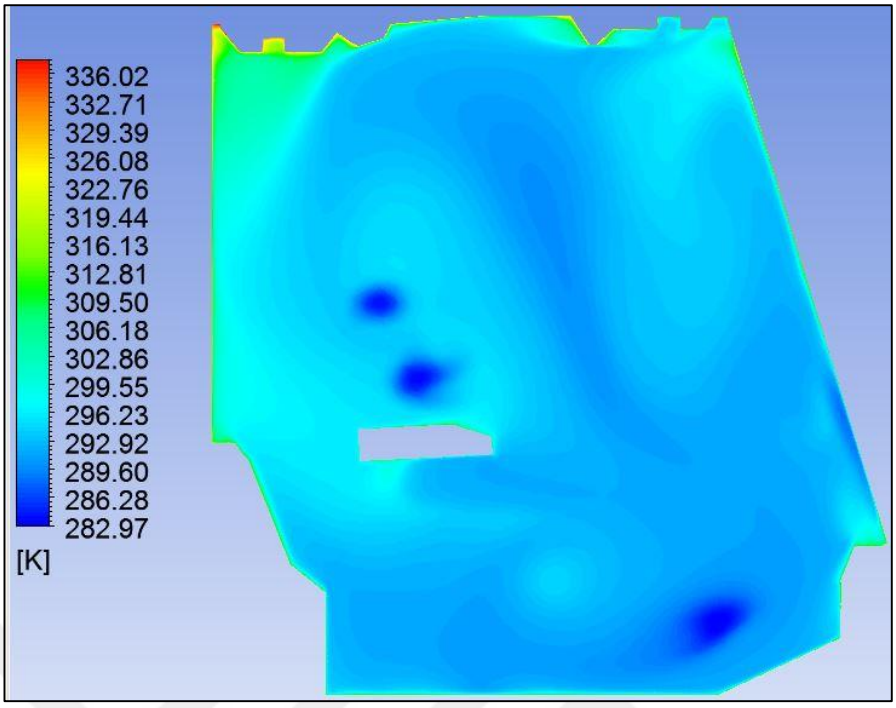

Figure 5.12 The temperature distribution of number 4 cross section

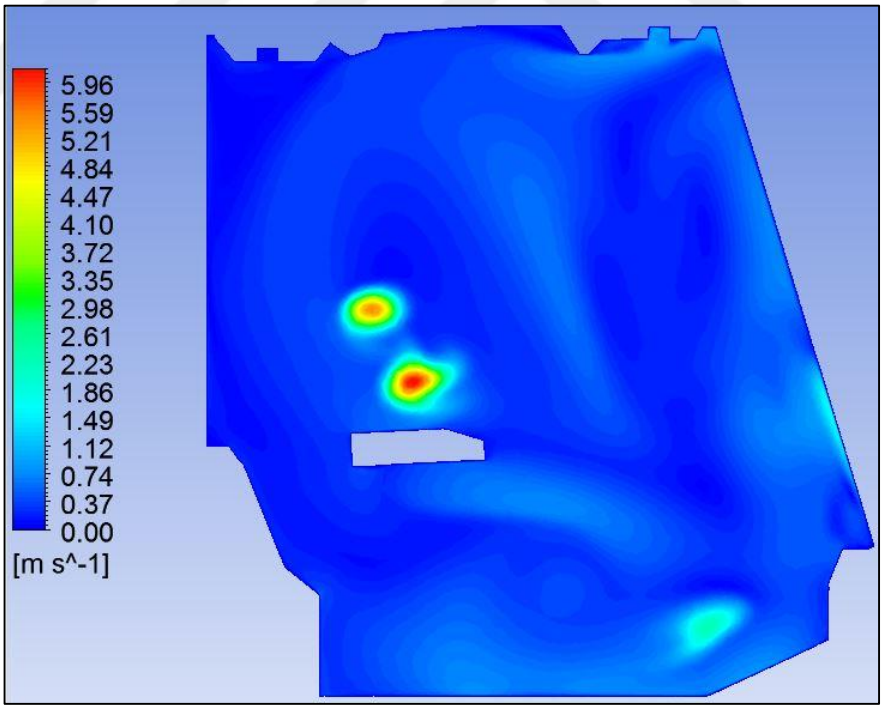

Figure 5.13 The airspeed distribution of number 4 cross section

Figure 5.11 illustrates the location of number 4 cross-section. *Figure 5.12* denotes the different temperature values of the number 4 cross-section between 9-43 °C. *Figure 5.13* illustrates the airspeed distributions on a plane. The average velocity in this plane is 0.85 m/s.

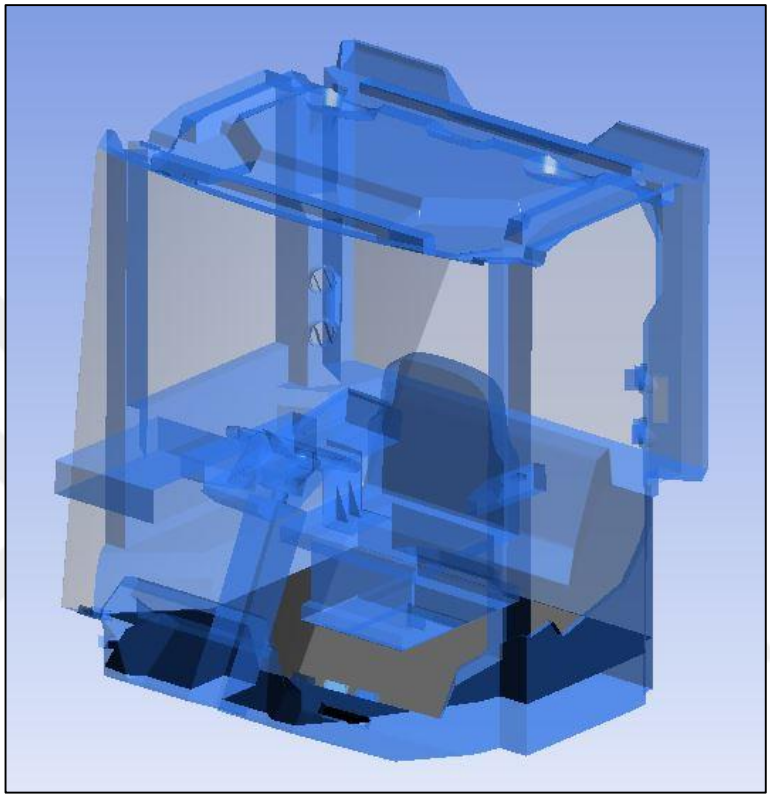

Figure 5.14 Position of the number 5 cross section

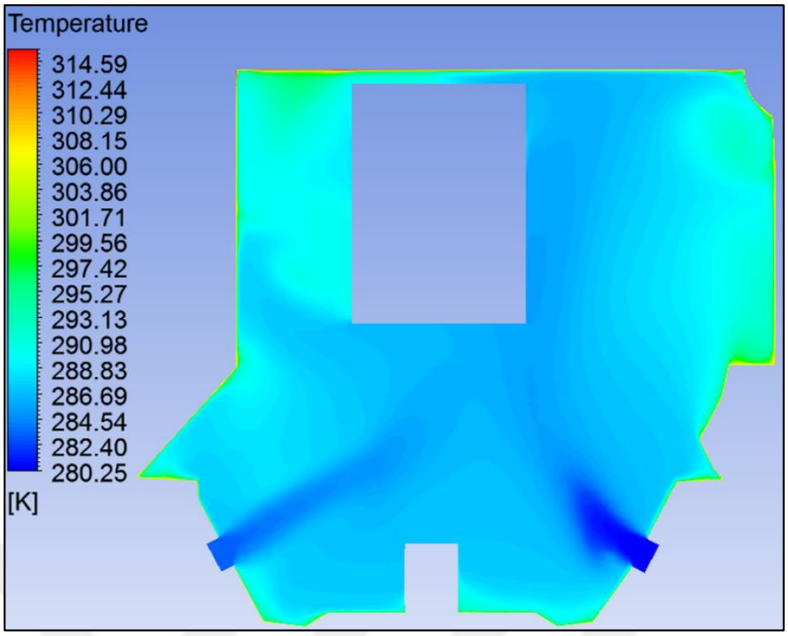

Figure 5.15 Temperature values of the operator at the foot level

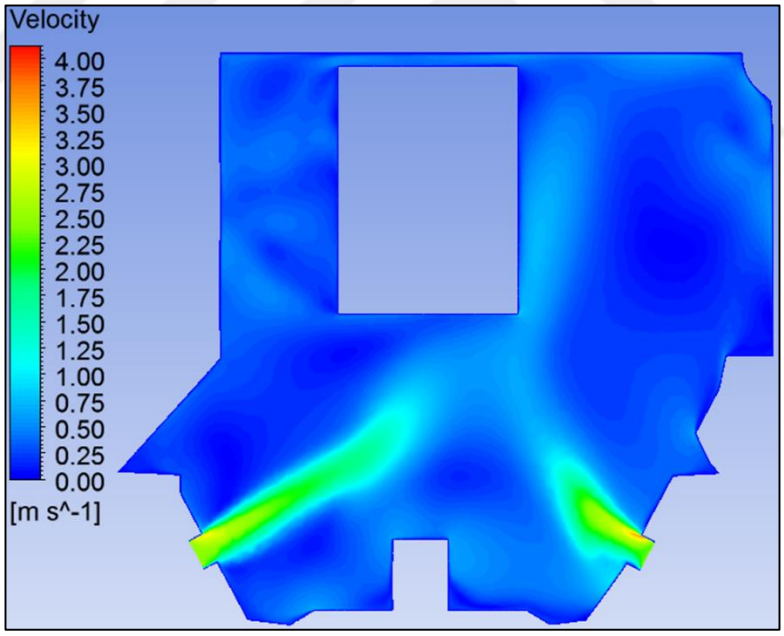

Figure 5.16 The airspeed distribution of the operator at the foot level

Figure 5.14 shows the location of number 5 cross-section. *Figure 5.15* demonstrates the different temperature values of the operator at the foot level between 18-20 °C. Figure *5.16* shows the airspeed distribution of the operator at the foot level.

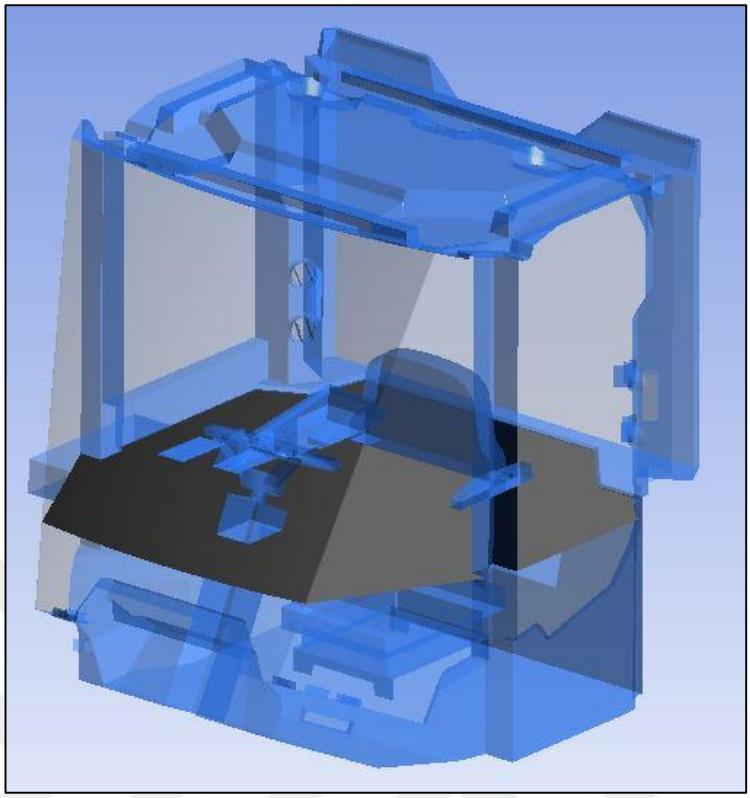

Figure 5.17 Position of the number 6 cross section

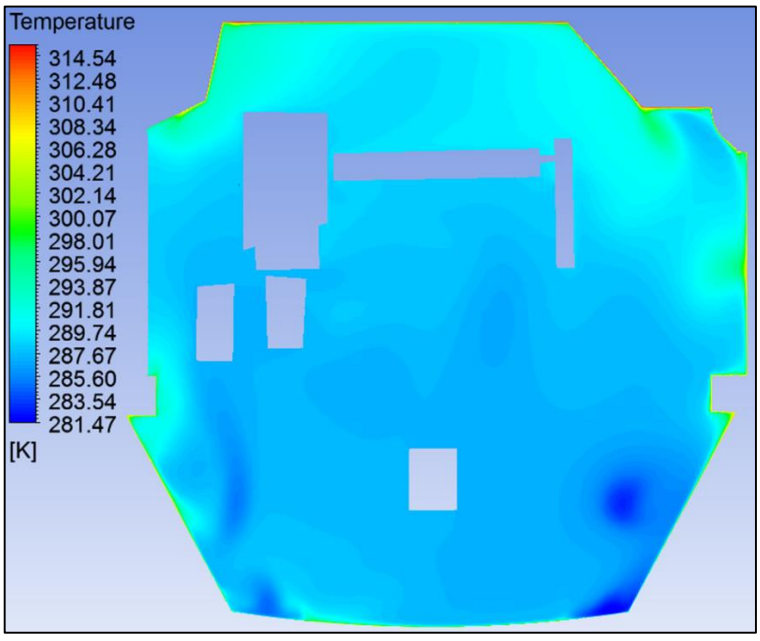

Figure 5.18 Temperature distribution of the operator in the chest position

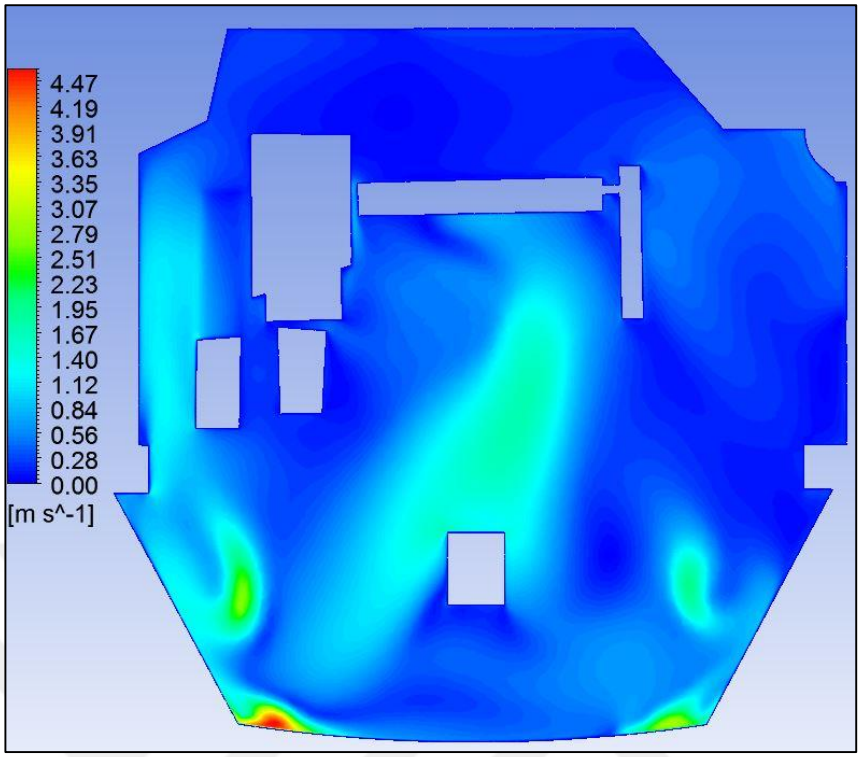

Figure 5.19 The airspeed distribution of the operator in the chest position

Figure 5.17 expresses the location of number 6 cross-section. *Figure 5.18* illustrates that the temperature distribution of the operator in the chest position changes within the range of 20-24 °C around the driver. A temperature variance of 5-6 °C between the temperature distributions has been determined on the right and left sides for the windshield position of the cabin. The cause for this difference can be considered to be the higher air velocity of the air vents close to the air conditioning fan unit accelerating the heat transfer in those areas. *Figure 5.19* shows airspeed distribution on a plane. It has been observed that air velocities vary locally.

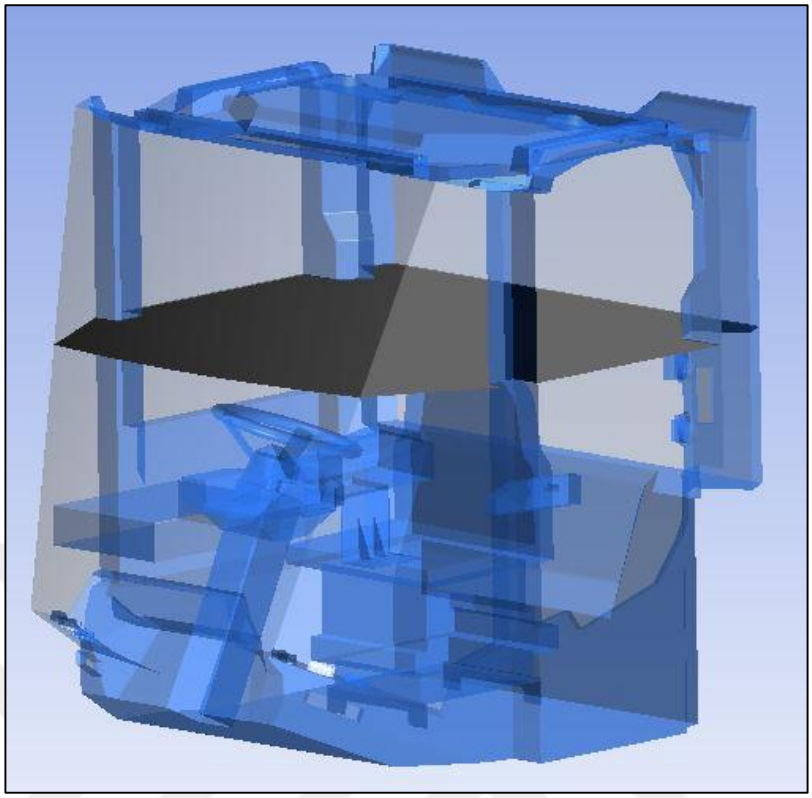

Figure 5.20 Position of the number 7 cross section

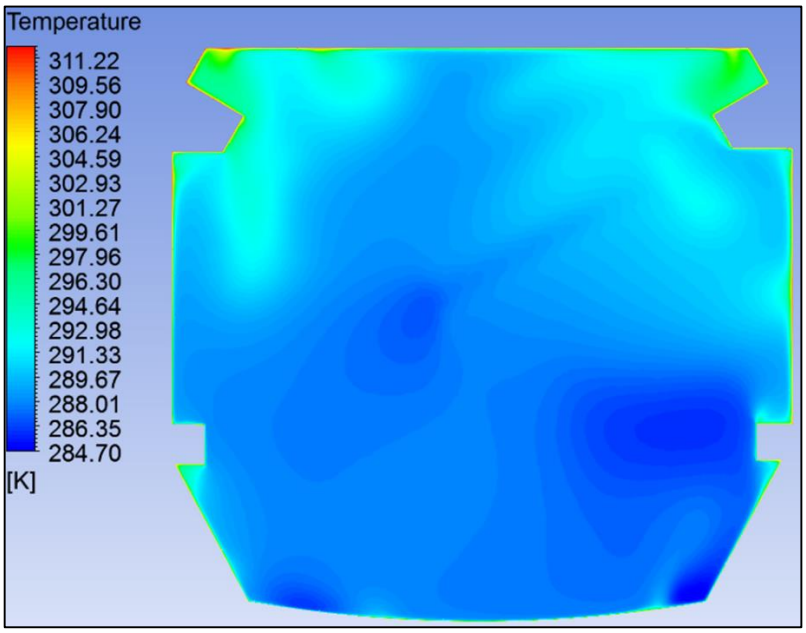

Figure 5.21 Temperature distribution of the operator's in head position

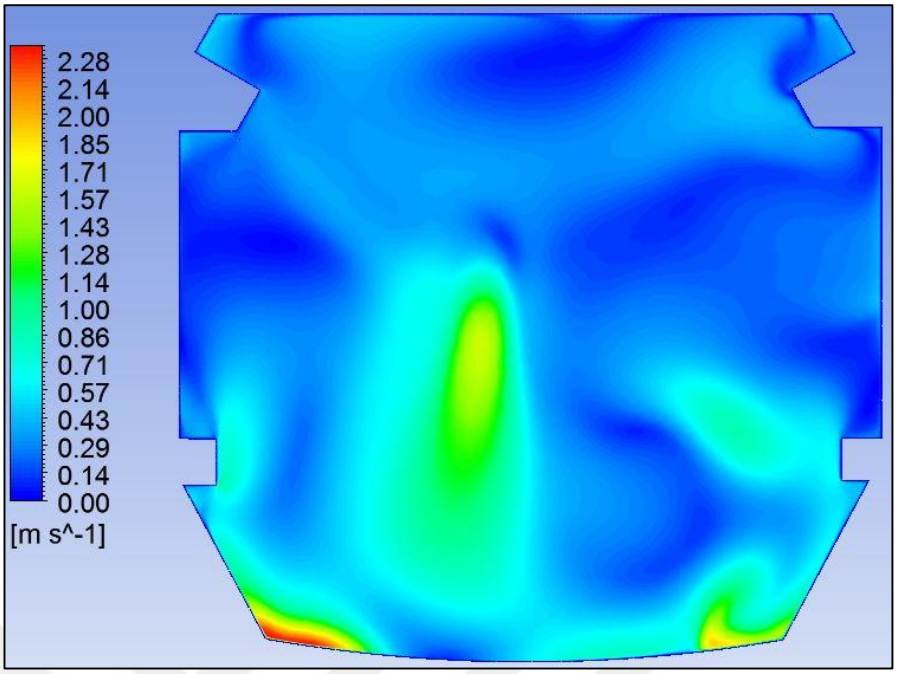

Figure 5.22 Airspeed distribution of the operator's in head position

Figure 5.20 shows the location of number 7 cross-section.

Figure 5.21, the temperature in the vent outlets varies between 6 and 11 °C while the temperature around the head of the operator is determined between 20-23 °C.

Figure 5.22 examines the velocity measurements in the operator head position, which are considered to be necessary. In the analysis, the air inlet positions have been directed directly to the operator, and the maximum velocities have been intended to be observed while the air conditioner was operating at full speed. The maximum value of the velocity around the operator's head was approximately 1.2 m/s. The result of the analysis in the eye around the operator was approximately 0.15 m/s.

5.2.2 The Second Analysis: Real Working Conditions

The second analysis has been performed using the verified CFD model obtained from the first analysis. The effects of solar radiation have also been included in this analysis. *Table 5.2* shows the differences between average experimental temperature measurement and average temperature CFD results for analysis.

Table 5.2 Differences between temperature measurement and analysis results for the second analysis

Points	Average temperature experimental results (K)	Average temperature CFD results (K)	Difference (°C)
Head position	296.15	298.4	2.25
Steering position	296.88	297.9	1.02
Right-arm position	295.4	294.9	0.5
Left-arm position	294.65	296.02	1.37
Right-foot position	292.35	293.1	0.75
Left-foot position	293	293.8	0.8

In the following figures, cross sections have been taken in different locations in order to be able to observe the temperature distributions in the machinery driver's cab.

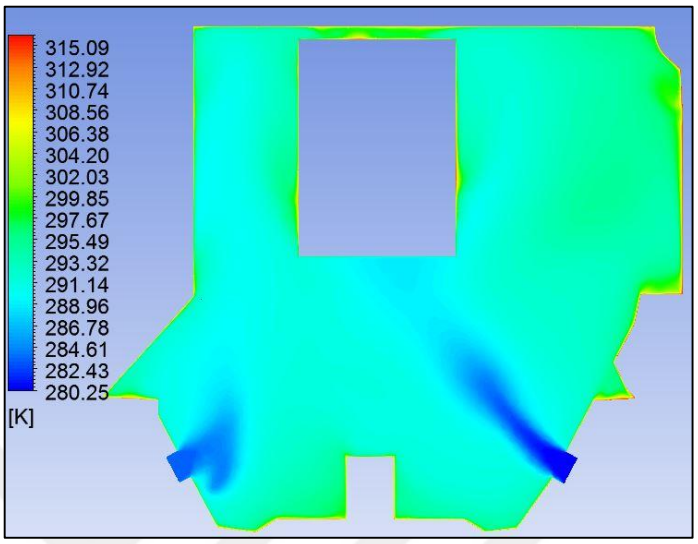

Figure 5.23 Temperature values of the operator at the foot level

Figure 5.23 demonstrates the different temperature values of the operator at the foot level between 20-22 °C. Due to the radiated heat, the temperature in the cabin wall close to the engine varies between 25-29 °C.

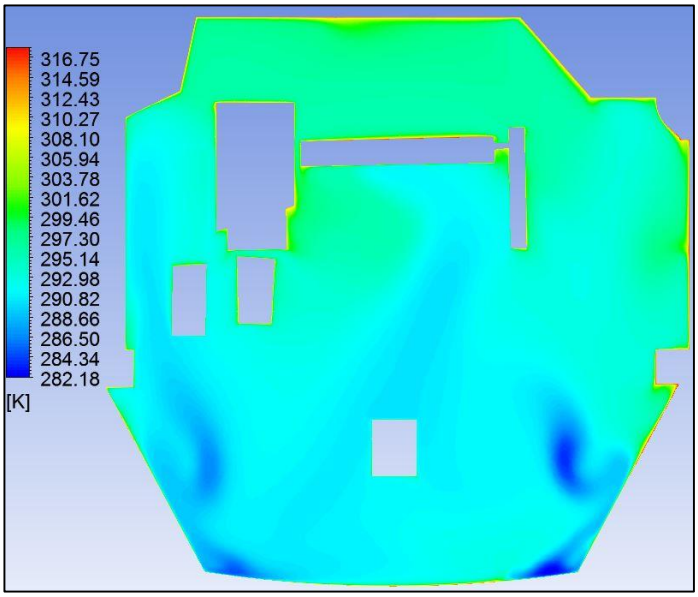

Figure 5.24 Temperature distribution of the operator in the chest position

Figure 5.24 illustrates that the temperature distribution of the operator in the chest position changes within the range of 21-26 °C around the driver. Due to the radiated heat, the temperature in the cabin walls varies between 27-32 °C.

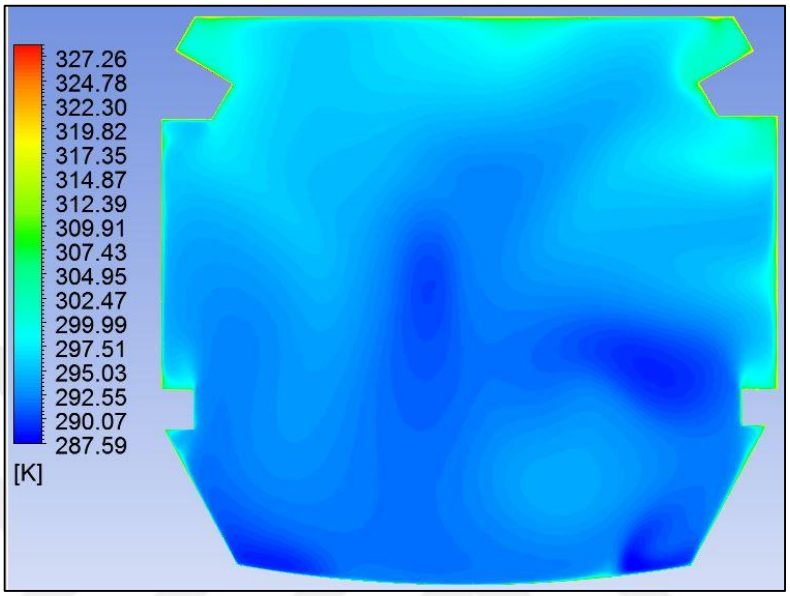

Figure 5.25 Temperature distribution of the operator's in head position

Figure 5.25, the temperature in the vent outlets varies between 6 and 12 °C while the temperature around the head of the operator is determined between 23-31 °C. A direct reflection of the solar load by the windshield at a certain angle and the different temperature and air velocities of the vents have caused this region to varying.

According to the results, differences have been observed in the accepted range (±3 °C) between the temperature results obtained from the test results and the temperature results obtained from the numerical analysis. The most important result to be obtained from this analysis is that using the verified CFD model from the previous analysis for a different analysis gives correct results. Even if conditions change, the difference between test and numerical analysis results is acceptable.

CHAPTER 6

CONCLUSION

The interior of the machinery driver’s cab is a very complex geometry compared to other indoor spaces because it has a smaller area and much higher air alteration velocities. So, creating an accurate CFD model can be rather complicated, given the need for verification and calibration compared to experimental data. In this thesis, flow analysis has been carried out for summer conditions by considering the velocity and temperature measurements taken from the air inlets in a machinery driver’s cab. The cooling problem in a machinery driver's cab has been examined as a numerically, and the data obtained have been compared with the experimental results. The model has been confirmed with a deviation of ± 3℃. The results have been indicated that the given boundary conditions have been close to reality. Besides the mesh size and solvent method have been appropriate for the computational model.

Another result that can be drawn from this study is that if utilized in a controlled manner, computational fluid dynamics has the potential to provide reliable results even if for complex systems such as air distribution systems.

The geometrical model investigated had a very complex structure and a simplified flow volume needs for numerical analysis. The creation of tiny size elements in the mesh stage is not desirable both as it extends the solution time and makes convergence difficult. So, it has been seen that it is significant to simplify the geometric model to be investigated with the aid of a drawing program as much as possible and to clean it from any unnecessary detail.

The calculation of surface view factors of the S2S radiation model takes a long time. Also, the mesh size can be in high quantity to obtain reliable and accurate results. For example, mesh independent size study has been done for this analysis. It has been seen that a supercomputer is needed to complete these studies successfully.

First of all, only the velocity distribution has been made according to the analysis process sequence. After the convergence of the velocity distribution, the energy module is turned on. As the final step, the radiation module has been turned on after the energy convergence is achieved. This process priority prevents the analysis from diverging or failing.

Another result is that the air distribution inside the cab is asymmetrical. In other words, it has been observed that there is low circulation of air in some locations while air flow is high in some places. Although modeling meets the test conditions, this situation may affect the comfort of the operator's environment. HVAC inlet-outlet configuration dramatically can influence temperature distributions inside a cab. Improvement of low air circulation zones can be significantly solved by changing air inlet/ air outlet designs. Also, further study is required to take into account all parameters that may impress HVAC system efficiency. For example, further research aimed at analyzing the actual role played by transient environmental parameters, such as radiant temperature, may also take into account parameters that may alter thermal comfort, such as inner surfaces, air velocity vibration, local air turbulence.

CFD offers new opportunities to learn knowledge acquisition about engineering fluid dynamics. The climate system can be thought of as two different sections: the air distribution system and the driver's compartment. In this thesis, only the driver compartment part was discussed. Studies are underway for the analysis that is included in both air distribution part and driver's cab for future studies.

Also, in later studies, the effect of solar load on non-opaque surfaces should be examined. Because FLUENT only deals with the solar load that affects transparent and semitransparent surfaces.

It should also be discussed how many points should be taken for model validation from within the driver's cab for future works.

Examining the topics mentioned above will be useful in terms of the development and optimization of the model.

REFERENCES

[1] Roy, D., Khoury, K. El., Clodic, D., & Petitjean, C. Modeling of in-vehicle heat transfers using a zonal approach. SAE Tech. Pap. Ser., 1 (1133), 9. 2010

[2] ISO 10263-4, Earth-Moving Machinery- Operator Enclosure Environment, Second edition, 2009

[3] Shah, A. B., Cless, C. M., Curlee, J. S., & Edmondson, J. Thermal analysis and simulations for optimizing HVAC load on heavy trucks. SAE Tech. Pap. Ser., 1 (2657), 11. 2010

[4] Aronson, D., Chroneer, Z., Elofsson, P., & Fellbom, H. Comparison between CFD and PIV measurements in a passenger compartment. SAE Tech. Pap. Ser., 1 (977), 10. 2010

[5] Flores, J., & Chaderjian, N. M. Zonal Navier-Stokes methodology for flow simulation about a complete aircraft. Journal of Aircraft, 27 (7), 583–590. 1990

[6] Wan, J. W., & Kooi, J. V. Influence of the position of supply and exhaust openings on comfort in a passenger vehicle. Int. J. Veh. Des., 12, 588–597, 1991

[7] Danca, P., Bode, F., Nastase, I., & Meslem, A. On the possibility of CFD modeling of the indoor environment in a vehicle. Energy Procedia, 112 (2017), 656–663. 2016.

[8] Alexandrov, A., Kudriavtsev, V., & Reggio, M. Analysis of flow patterns and heat transfer in generic passenger car mini-environment managing director. 9th Annual Conference of the CFD Society of Canada, 5. 2001

[9] Liu, H. Simulation and optimization of indoor thermal environment in a ship air-conditioning system. Procedia Environ. Sci., 11 (2011), 1055–1063. 2011

[10] Axelsson, N., & Enwald, H. Accuracy in flow simulations of climate control-part 1: the air distribution system. SAE Tech. Pap. Ser., 1 (1200), 12. 1999

[11] Chronéer, Z., & Axelsson, N. Accuracy in flow simulations of climate control - part 2: the passenger compartment. SAE Tech. Pap. Ser., 1 (1201), 10. 2010

[12] Currle, J., & Maué, J. Numerical study of the influence of air vent area and air mass flux on the thermal comfort of car occupants. SAE Tech. Pap. Ser., 1 (980), 10. 2000

[13] Aliahmadipour, M., Abdolzadeh, M., & Lari, K. Airflow simulation of the HVAC system in the compartment of a passenger coach. Appl. Therm. Eng., 123, 973–990. 2017

[14] Akdemir, S. Bir traktör kabininde ortam şartlarının yaz koşullarında HAD ile belirlenmesi. Journal of Tekirdag Agricultural Faculty, 13 (02), 46-54. 2016

[15] Akdemir, S., Oğuz, E., Öztürk, S., & Ülger, P. Soğuk hava depolarında ortam koşullarının hesaplamalı akışkanlar dinamiği (CFD) ile modellenmesi. Journal of Agricultural Machinery Science, 8 (2), 241–248. 2012

[16] Aroussi, A., Hassan, A., & Morsi, Y. S. Numerical simulation of the airflow over and heat transfer through a vehicle windshield defrosting and demisting system. Heat Mass Transfer and Stoffuebertragung, 401–405. 2003

[17] AKYOL, Ş. M. Otomobil kabininde farklı koşullarda ısıl konforun değişiminin incelenmesi. Yayınlanmamış yüksek lisans tezi, Uludağ Üniversitesi Fen Bilimleri Enstitüsü. 2008

[18] Conceição, E. Z. E., Silva, M. C. G., André, J. C. S., & Viegas, D. X. A computational model to simulate the thermal behavior of the passenger's compartment of vehicles. SAE Tech. Pap. Ser., 1 (778), 1483–1492. 1999

[19] Çengel, Y., & Cimbala, J.M. *Fluid mechanics fundamentals, and applications* (3rd Ed.). NY: Mc Graw-Hill Science Engineering Math. 2013

[20] Kundu, P. K., & Cohen, I. M. *Fluid Mechanics* (2nd Ed.). California: Elsevier Science. 2004

[21] Control Volume. (n.d.) retrieved from https://www.engineersedge.com/fluid_flow/control_volume.htm.

[22] Anderson, J. D. *Philosophy of computational fluid dynamics*. NY: McGraw-Hill. 1995

[23] White, F. M. *Viscous Fluid Flow* (3rd Ed.). NY: McGraw-Hill. 1974

[24] Tritton, D. J. *Physical fluid dynamics*. NY: Van Nostrand Reinhold Company, 1977

[25] Kuzmin, D. Introduction to computational fluid dynamics. Retrieved April 5, 2019, from http://www.mathematik.unidortmund.de/~kuzmin/cfdintro/cfd.html. 2010

[26] Incropera, D. P., Lavine, F. P., & DeWitt, A. S. *Fundamentals of heat and mass transfer* (6th Ed.). New Jersey: John Wiley & Sons. 2011

[27] ANSYS FLUENT User's Guide version R1, 2019

[28] Craft, T. J. *Wall functions, turbulence modeling for CFD*. Retrieved April 20, 2019, from http://cfd.mace.manchester.ac.uk/twiki/pub/Main/TimCraftNotes_All_Access/

advtm-wallfns.pdf. 2010

[29] Péric, M., & Ferziger, J. H. *Computational Methods for Fluid Dynamics* (3rd Ed.). 2002

[30] *Directional hotwire probe*. Retrieved May 21, 2019, from https://www.deltaohminternational.com/probes/ap471s1-directional-hotwire-probe-to-measure-air-speed-in-the-range-0140m-s-and-air-temperature-in-the-range-250c-800c. 2019

[31] *Vane probe with a thermocouple*. Retrieved May 21, 2019, from https://www.deltaohm.com/en/product/ap-472s1-vane-probe-with-thermocouple/. 2019

[32] *Type K Thermocouple*. Retrieved May 21, 2019, from https://www.thermocoupleinfo.com/type-k-thermocouple.htm.

[33] Finstuen, B. E. *Solar Energy*. Retrieved May 21, 2019, from https://www.solarpowerworldonline.com/2016/07/projects-need-pyranometers/. 2010

CURRICULUM VITAE

PERSONAL INFORMATION

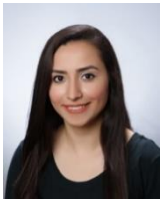

Name Surname **:** Hazal KOYUNCU
Date of Birth **:** 13.04.1992
Phone **: -**
E-mail **:** hzl_kync@hotmail.com

EDUCATION

High School **:** Alparslan Anatolian High School (2006 -2010)
Bachelor **:** Ankara Yildirim Beyazit University (2011-2016)
Master Degree **:** Ankara Yildirim Beyazit University (2016 – 2019)

WORK EXPERIENCE

HİDROMEK A.Ş.
Analysis Engineer (2017- continued)